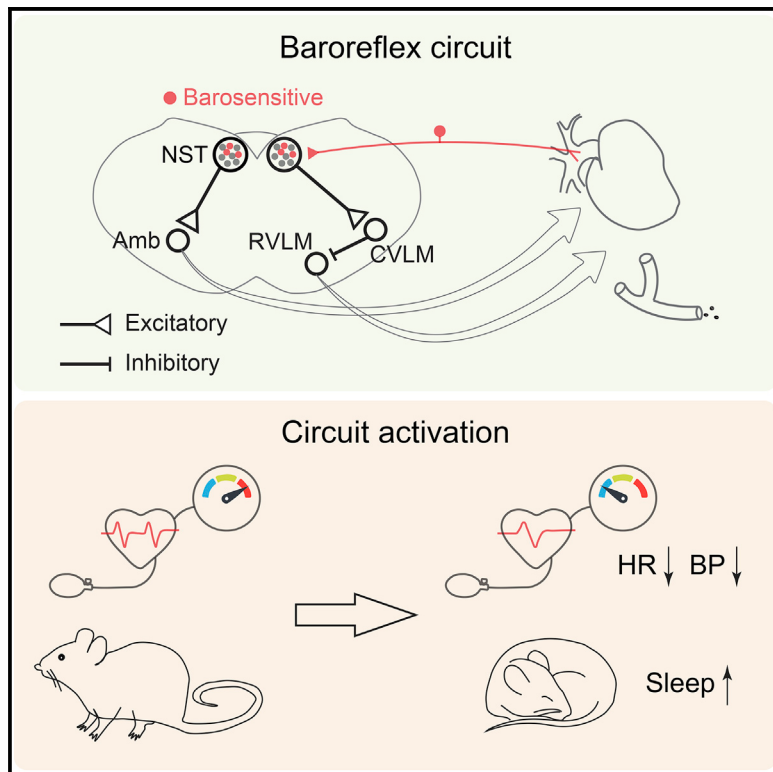


## Cardiovascular baroreflex circuit moonlights in sleep control

### Graphical abstract



### Authors

Yuanyuan Yao, Zeke Barger,  
Mohammad Saffari Doost, ...,  
Shenqin Yao, Hongkui Zeng, Yang Dan

### Correspondence

ydan@berkeley.edu

### In brief

Yao et al. show that the activity of neurons at key stages of baroreflex pathways in the mouse brain stem promotes sleep in addition to decreasing the blood pressure and heart rate, indicating that a basic circuit for autonomic cardiovascular control is also integral to sleep-wake brain-state regulation.

### Highlights

- Activity-dependent genetic labeling of barosensitive neurons in mouse NST
- Activation of NST barosensitive neurons promotes non-REM sleep
- Activation of CVLM GABAergic neurons in vasomotor pathway promotes non-REM sleep
- Activation of Amb cholinergic neurons in cardiac pathway promotes non-REM sleep



## Article

# Cardiovascular baroreflex circuit moonlights in sleep control

Yuanyuan Yao,<sup>1</sup> Zeke Barger,<sup>1</sup> Mohammad Saffari Doost,<sup>1</sup> Chak Foon Tso,<sup>1,3</sup> Dana Darmohray,<sup>1</sup> Daniel Silverman,<sup>1</sup> Danqian Liu,<sup>1,4</sup> Chenyan Ma,<sup>1</sup> Ali Cetin,<sup>2,5</sup> Shenqin Yao,<sup>2</sup> Hongkui Zeng,<sup>2</sup> and Yang Dan<sup>1,6,\*</sup>

<sup>1</sup>Division of Neurobiology, Department of Molecular and Cell Biology, Helen Wills Neuroscience Institute, Howard Hughes Medical Institute, University of California, Berkeley, Berkeley, CA 94720, USA

<sup>2</sup>Allen Institute for Brain Science, Seattle, WA, USA

<sup>3</sup>Present address: Dascena, Inc., Oakland, CA, USA

<sup>4</sup>Present address: Center for Excellence in Brain Science and Intelligence Technology, Institute of Neuroscience, Chinese Academy of Sciences, Shanghai, P.R. China

<sup>5</sup>Present address: CNC Program, Stanford University, Palo Alto, CA, USA

<sup>6</sup>Lead contact

\*Correspondence: ydan@berkeley.edu

<https://doi.org/10.1016/j.neuron.2022.08.027>

## SUMMARY

Sleep disturbances are strongly associated with cardiovascular diseases. Baroreflex, a basic cardiovascular regulation mechanism, is modulated by sleep-wake states. Here, we show that neurons at key stages of baroreflex pathways also promote sleep. Using activity-dependent genetic labeling, we tagged neurons in the nucleus of the solitary tract (NST) activated by blood pressure elevation and confirmed their barosensitivity with optrode recording and calcium imaging. Chemogenetic or optogenetic activation of these neurons promoted non-REM sleep in addition to decreasing blood pressure and heart rate. GABAergic neurons in the caudal ventrolateral medulla (CVLM)—a downstream target of the NST for vasomotor baroreflex—also promote non-REM sleep, partly by inhibiting the sympathoexcitatory and wake-promoting adrenergic neurons in the rostral ventrolateral medulla (RVLM). Cholinergic neurons in the nucleus ambiguus—a target of the NST for cardiac baroreflex—promoted non-REM sleep as well. Thus, key components of the cardiovascular baroreflex circuit are also integral to sleep-wake brain-state regulation.

## INTRODUCTION

The transition from wakefulness to sleep is associated with profound changes in both the brain state and motor activity of the animal. In addition to decreases in somatic motor activity and skeletal muscle tone, there is also a strong reduction of autonomic motor activity, leading to a lower blood pressure, slower heart rate, and other physiological changes (Benarroch, 2018; Conway et al., 1983; Silvani and Dampney, 2013; Somers et al., 1993). Sleep deficits are known to contribute significantly to cardiovascular diseases such as hypertension and coronary heart disease (Tobaldini et al., 2017). However, the mechanistic link between sleep and cardiovascular health remains poorly understood, especially at the neural circuit level.

An important neural mechanism for cardiovascular regulation is the baroreflex, a negative feedback loop in which an increase in arterial blood pressure sensed by peripheral baroreceptors is transmitted to the medullary nucleus of the solitary tract (NST), which triggers compensatory changes in both cardiac and vaso-motor activity to reduce the blood pressure (Dampney, 2016; Guyenet, 2006). There are two essential pathways for baroreflex:

the glutamatergic projection from the NST to the nucleus ambiguus (Amb) activates the cholinergic preganglionic parasympathetic neurons, which leads to a decrease in the heart rate; the NST glutamatergic projection to the caudal ventrolateral medulla (CVLM) activates the GABAergic neurons, which in turn inhibit sympathoexcitatory adrenergic neurons in the rostral ventrolateral medulla (RVLM), resulting in a reduction of the vasomotor tone and blood pressure.

Baroreflex is known to be modulated by sleep-wake brain states (Benarroch, 2018; Silvani et al., 2015; Silvani and Dampney, 2013). For example, some studies showed that during non-REM (NREM) sleep, the baroreflex set point is significantly lower than during wakefulness but the sensitivity (measured by the slope of linear regression between the heart rate decrease and blood pressure increase) is higher; both of these changes are likely to contribute to the decrease in blood pressure (Conway et al., 1983; Smyth et al., 1969; Tang and Dworkin, 2010). The effects of brain states on baroreflex are likely mediated by inputs from the midbrain and forebrain regions such as the periaqueductal gray and hypothalamus, both of which contain sleep-wake regulating neurons (Benarroch, 2018; Scammell



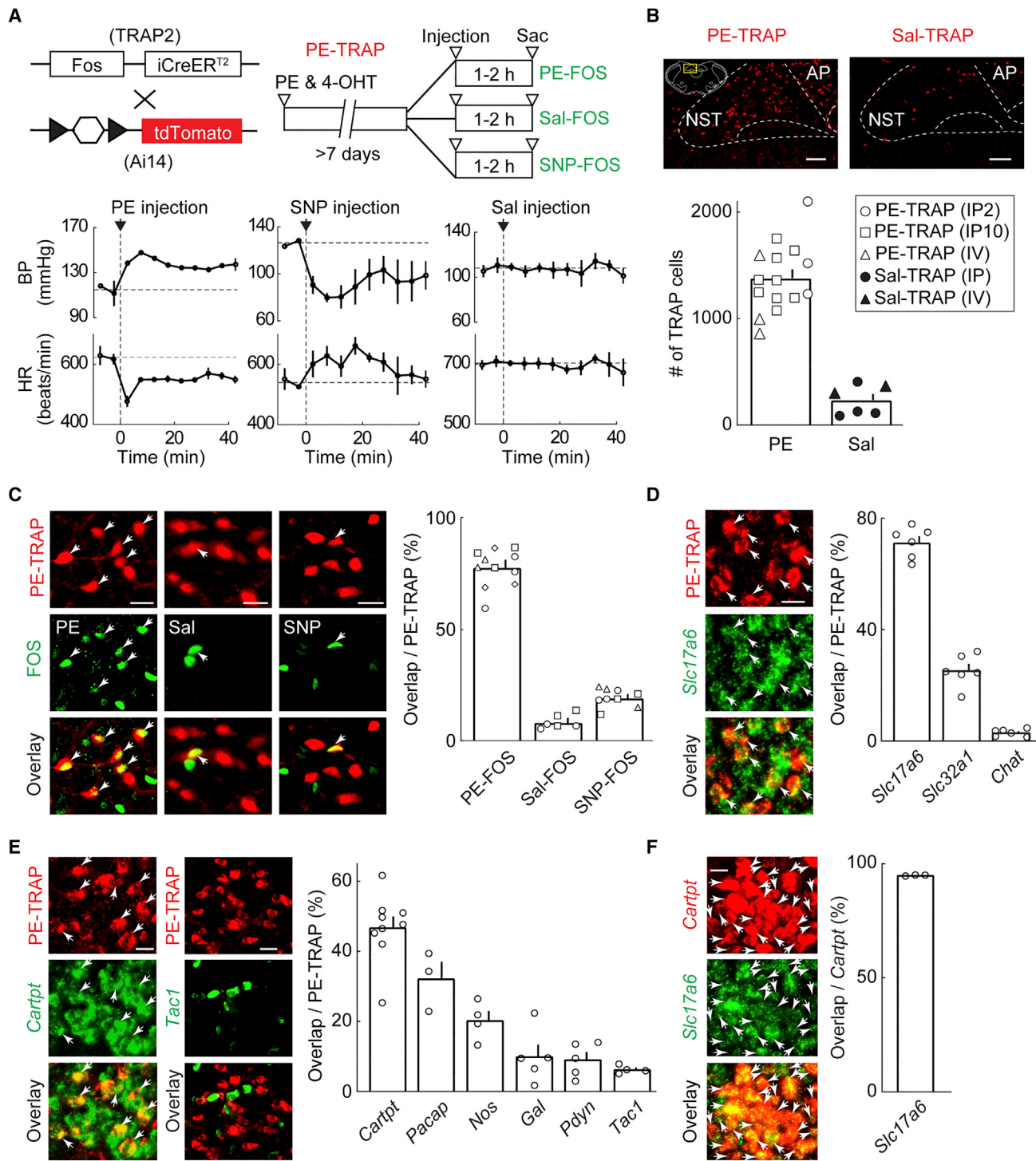


**Figure 1. Activity-dependent genetic labeling of NST barosensitive neurons**

(A) Top: experimental schematic. Mice expressing CreER under the Fos promoter (TRAP2) were crossed with Cre-inducible reporter mice expressing tdTomato or eGFP. PE and 4-OHT were injected to label neurons activated by blood pressure elevation; >7 days later they were injected a second time with PE, saline (Sal), or SNP and sacrificed 40 min–2 h later for Fos immunohistochemistry. Bottom: blood pressure (BP) and heart rate (HR) changes following PE (10 mg/kg), SNP (0.6 mg/kg), and saline injection for the TRAP experiment. Error bars,  $\pm$ SEM; n = 3 mice for each group. Vertical dashed lines and arrowheads indicate injection time. Horizontal dashed lines indicate mean values before injection.

(B) Top: tdTomato-expressing neurons in the NST (rectangle in coronal diagram) in PE-TRAP and Sal-TRAP mice (4-OHT paired with saline injection). Scale bars, 100  $\mu$ m. Bottom: average number of tdTomato-/eGFP-expressing NST neurons in PE-TRAP and Sal-TRAP mice. Open circle, IP injection of 2 mg/kg PE (n = 3

(legend continued on next page)

et al., 2017; Silvani et al., 2015; Silvani and Dampney, 2013; Zhang et al., 2019; Zhong et al., 2019). However, it is unclear whether the neural circuits dedicated to cardiovascular regulation can affect brain states in return. Although decades ago there were some reports that mechanical or electrical stimulation of baroreceptors in the periphery could induce sleep-like states (Bonvallet et al., 1954; Bridgers et al., 1985; Dell and Padel, 1965; Dell and Marillau, 1966; Koch, 1932; Mazzella et al., 1957; Padel and Dell, 1965), the effects were thought to be limited to anesthetized conditions (Silvani et al., 2015) and the underlying circuit mechanism remained unknown.

In this study, we show that the cardiovascular baroreflex circuit contributes strongly to sleep regulation in freely moving mice. Using activity-dependent genetic labeling (Allen et al., 2017; Guenthner et al., 2013), we tagged NST neurons activated by pharmacologically induced blood pressure elevation and confirmed their barosensitivity with optrode recording and calcium imaging. Chemogenetic or optogenetic activation of the tagged NST neurons promoted NREM sleep in addition to decreasing the blood pressure and heart rate. Activation of their projection targets—the CVLM → RVLM vasomotor pathway and the Amb cardiac pathway—also promoted NREM sleep. These results indicate that the baroreflex circuit, previously thought to be a basic feedback mechanism for cardiovascular homeostasis, also contributes to sleep-wake brain state regulation.

## RESULTS

### Activity-dependent genetic labeling of NST barosensitive neurons

To test genetic labeling of barosensitive neurons, we crossed the TRAP2 mouse line expressing tamoxifen-inducible Cre recombinase under the Fos promoter (Allen et al., 2017; Guenthner et al., 2013) with a reporter mouse line expressing tdTomato or eGFP (Figure 1A). Baroreceptors were activated by injecting phenylephrine (PE, intraperitoneal or intravenous), a vasoconstrictor (acting on adrenergic receptors in blood vessels) commonly used for identifying barosensitive neurons (Chan and Sawchenko, 1998; Dampney et al., 2003). PE injection indeed caused an increase in arterial blood pressure and a concomitant decrease in heart rate (Figure 1A), indicating activation of the baroreflex. The injection of 4-hydroxytamoxifen (4-OHT, 20 mg/kg) at the same time allowed the Cre estrogen receptor (CreER) expressed in PE-activated neurons to enter the nucleus and turn on tdTomato/eGFP expression. After >7 days, we found many tdTomato-/eGFP-labeled neurons in the NST (referred to as “NST<sup>PE-TRAP</sup> neurons,” Figures 1B and S1A). Immunohistochemical staining of c-Fos 40 min–2 h after another injection

confirmed that the vast majority of NST<sup>PE-TRAP</sup> neurons were activated by PE (Figure 1C), but very few were activated by the injection of saline or sodium nitroprusside (SNP, 0.6 mg/kg), which decreased the blood pressure through nitric-oxide-induced relaxation of vascular smooth muscles (Figure 1A). This indicates a high specificity of PE-TRAP labeling in the NST.

Fluorescence *in situ* hybridization showed that the majority ( $71.3\% \pm 2.3\%$ , mean  $\pm$  SEM) of NST<sup>PE-TRAP</sup> neurons expressed the glutamatergic marker vesicular glutamate transporter 2 (encoded by *Slc17a6*), and only  $25.3\% \pm 2.3\%$  expressed the GABAergic/glycinergic marker *Slc32a1*; very few NST<sup>PE-TRAP</sup> neurons expressed *Chat*, a cholinergic marker heavily expressed in the dorsal motor nucleus of the vagus, just ventral to the NST (Figure 1D). Among other markers that are highly expressed in the caudal NST (based on a survey of the Allen Mouse Brain Atlas ISH dataset), cocaine- and amphetamine-regulated transcript (CART, encoded by *Cartpt*) is expressed in a large fraction ( $46.8\% \pm 3.2\%$ ) of NST<sup>PE-TRAP</sup> neurons (Figures 1E and S1B); the great majority ( $94.9\% \pm 0.1\%$ ) of NST *Cartpt*<sup>+</sup> neurons are glutamatergic (Figure 1F).

In addition to an increase in blood pressure, PE injection could induce other physiological changes, which may be responsible for the labeling of some of the NST<sup>PE-TRAP</sup> neurons. To further verify the barosensitivity of NST<sup>PE-TRAP</sup> neurons, we tagged them with ChR2 and made optrode recordings of their spiking activity together with blood pressure and heart rate measurements in freely moving mice (Figure 2A). High-frequency laser pulse trains (15 and 30 Hz, 10 ms per pulse, 16 pulses/train) were applied intermittently, and single units showing reliable laser-evoked spikes at short latencies were identified as ChR2-tagged NST<sup>PE-TRAP</sup> neurons (Figure S2A) (Anikeeva et al., 2011). As shown in the example recording in Figure 2B, both the blood pressure and heart rate fluctuated over time, and the firing rate of the identified neuron closely followed the blood pressure changes. When analyzed on a timescale of seconds (e.g., using 5-s time bins), 15/19 (78.9%) identified NST<sup>PE-TRAP</sup> neurons (from 9 mice) were positively correlated with the blood pressure at the level of  $p < 0.01$ , whereas only 17/42 (40.5%) unidentified NST neurons showed a positive correlation (Figure 2C). On a shorter, subsecond timescale, 12/19 identified neurons showed spiking activity significantly time-locked to the heartbeat (Figure 2D) (Balan Júnior et al., 2004; Hayward and Felder, 1995; Rogers et al., 1993), suggesting that they were also sensitive to the pulsatile blood pressure change within a single cardiac cycle. In a subset of the recordings, we further tested the acute effect of PE injection (0.5 mg/kg). Within a few seconds, these neurons showed firing rate increases concomitant with the rise in blood pressure (Figures 2E and S2D). Thus, the NST<sup>PE-TRAP</sup> neurons

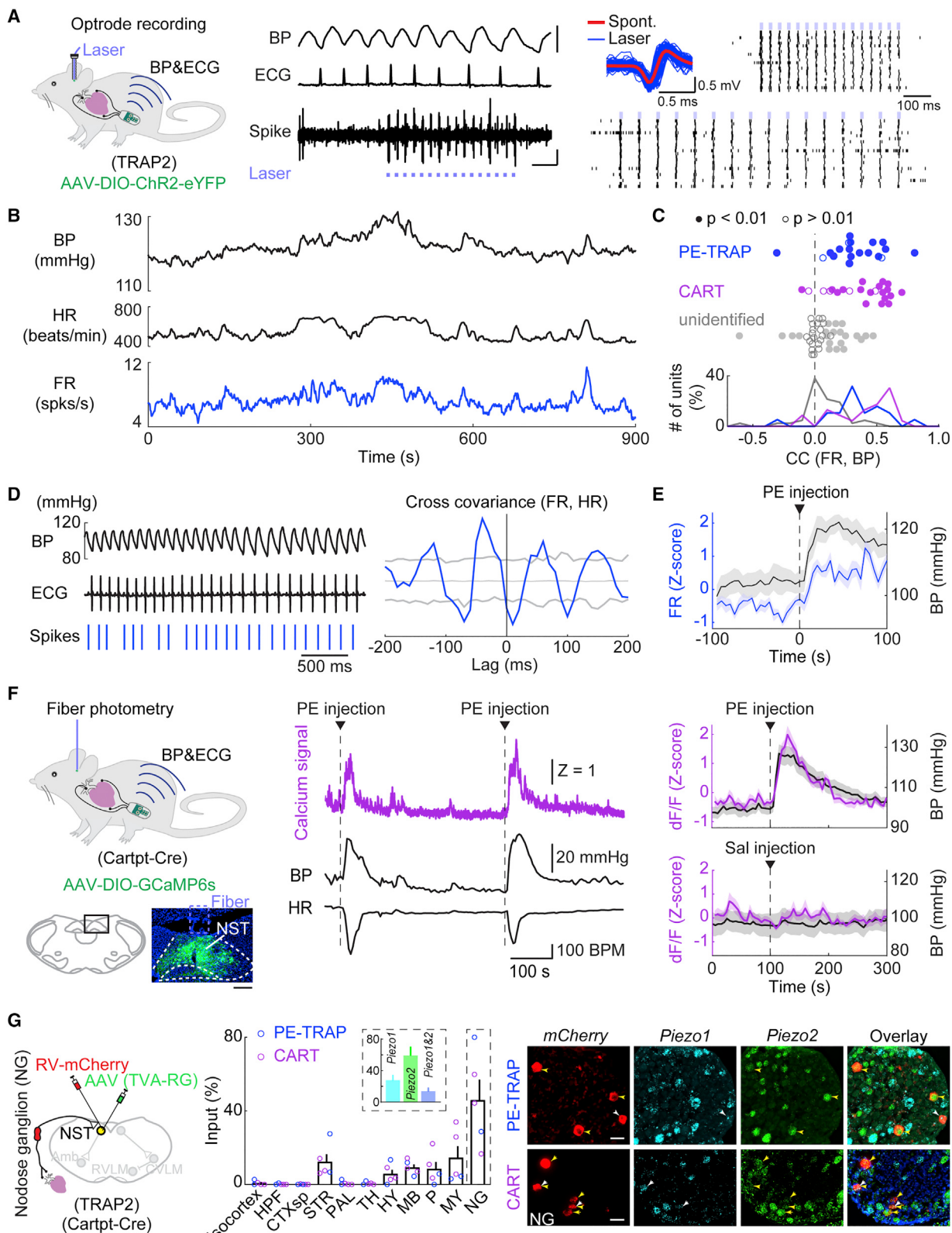
(mice); open square, IP injection of 10 mg/kg PE ( $n = 9$ ); open triangle, IV infusion of PE ( $n = 3$ ); filled circle, IP injection of saline ( $n = 4$ ); filled triangle, IV infusion of saline ( $n = 2$ ). Error bar,  $\pm$ SEM. AP, the area postrema.

(C) Overlap between PE-TRAP and PE-, Sal-, or SNP-induced Fos expression in NST. Arrowheads indicate co-labeled neurons. Scale bars, 20  $\mu$ m. Right: percentages of PE-TRAP neurons that express Fos induced by PE, Sal, or SNP. Triangle: PE-TRAP (IV); square: PE-TRAP (IP, 10 mg/kg); circle: PE-TRAP (IP, 2 mg/kg); diamond: PE-TRAP (IP, 2 mg/kg, but with PE-TRAP performed in dark phase and Fos in light phase). Error bar,  $\pm$ SEM.

(D) Overlap between PE-TRAP and cell type markers, *Slc17a6* (glutamatergic), *Slc32a1* (GABAergic/glycinergic), and *Chat* (cholinergic) shown by double FISH. Scale bars, 20  $\mu$ m. Error bars,  $\pm$ SEM.

(E) Overlap between PE-TRAP and several other markers, *Cartpt* ( $n = 9$  mice), *Pacap* (pituitary adenylate-cyclase-activating polypeptide,  $n = 3$ ), *Nos* (nitric oxide synthase 1,  $n = 4$ ), *Gal* (galanin,  $n = 5$ ), *Pdyn* (prodynorphin,  $n = 5$ ), and *Tac1* (tachykinin precursor 1,  $n = 4$ ). Scale bars, 20  $\mu$ m. Error bars,  $\pm$ SEM.

(F) Overlap between *Cartpt* and *Slc17a6* ( $n = 3$  mice). Scale bars, 20  $\mu$ m. Error bars,  $\pm$ SEM.



(legend on next page)

are sensitive to blood pressure changes on subsecond to second timescales, an important property for the rapid feedback in baroreflex. Note, however, that the labeling efficiency of the current method is not 100% (Allen et al., 2017), and the  $\text{NST}^{\text{PE-TRAP}}$  population is likely a subset of barosensitive  $\text{NST}$  neurons.

Because many  $\text{NST}^{\text{PE-TRAP}}$  neurons expressed CART (Figure 1E), we also made optrode recordings from the CART neuron population using Cartpt-Cre mice (Figure S2C). Similar to  $\text{NST}^{\text{PE-TRAP}}$  neurons, 17/23 identified  $\text{NST}^{\text{CART}}$  neurons (from 9 mice) showed firing rates positively correlated with the blood pressure fluctuations on the timescale of seconds (Figures 2C and S2B) and 11/23 of them were time-locked to the heartbeat on the subsecond timescale. Calcium imaging through fiber photometry also showed that  $\text{NST}^{\text{CART}}$  neuron activity increased concomitantly with the blood pressure elevation induced by PE injection (Figure 2F). Rabies-mediated retrograde transsynaptic tracing (Miyamichi et al., 2011; Wickersham et al., 2007) from  $\text{NST}^{\text{PE-TRAP}}$  or  $\text{NST}^{\text{CART}}$  neurons revealed direct inputs from neurons in the nodose ganglion expressing Piezo1 and 2 (Figure 2G), a population that contain baroreceptors (Min et al., 2019; Zeng et al., 2018). Thus, some of the  $\text{NST}^{\text{PE-TRAP}}$  and  $\text{NST}^{\text{CART}}$  neurons likely receive direct excitatory inputs from baroreceptors, while others may be activated indirectly through polysynaptic pathways.

### Activation of $\text{NST}$ barosensitive neurons promotes NREM sleep

We next tested the effects of chemogenetic activation of  $\text{NST}^{\text{PE-TRAP}}$  neurons on both the cardiovascular activity and brain state in freely moving mice with simultaneous electroencephalogram (EEG), electromyogram (EMG), arterial blood pressure, and electrocardiogram (ECG) recordings (Figures 3A and S3A). In mice expressing hM3D(Gq)-mCherry in  $\text{NST}^{\text{PE-TRAP}}$  neurons, clozapine-N-oxide (CNO) injection (0.1 mg/kg) caused

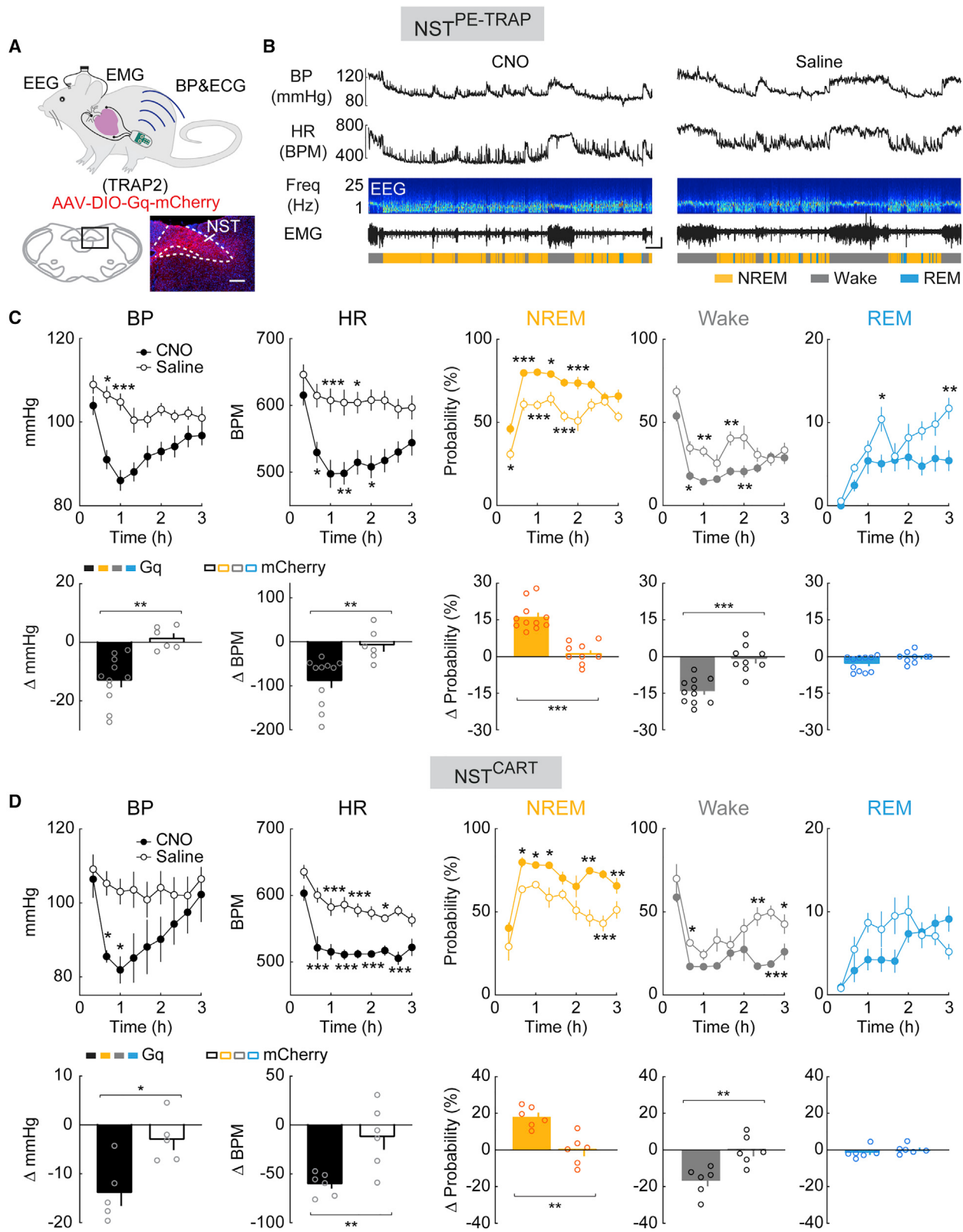
strong decreases in both the blood pressure and heart rate (Figures 3B and 3C), consistent with the known function of  $\text{NST}$  barosensitive neurons in cardiovascular regulation (Dampney, 2016; Guyenet, 2006). Importantly, CNO injection also induced a significant increase in NREM sleep and decrease in wakefulness, as measured by EEG and EMG recordings (Figures 3B and 3C). In control mice expressing mCherry alone, CNO had no significant effect (Figure S3B), and the CNO-induced changes were significantly different between the hM3D(Gq) and control mice (Figure 3C). In a second control experiment, we tested the effect of chemogenetic activation of  $\text{NST}^{\text{Sal-TRAP}}$  neurons (labeled with hM3D(Gq)-mCherry after saline instead of PE injection). CNO injection also caused no significant change in blood pressure, heart rate, or brain states (Figure S3C).

We then tested the effects of activating the CART neuron population using Cartpt-Cre mice. Similar to  $\text{NST}^{\text{PE-TRAP}}$  neurons, chemogenetic activation of  $\text{NST}^{\text{CART}}$  neurons promoted NREM sleep in addition to decreasing the blood pressure and heart rate (Figures 3D, S4A, and S4D). In contrast, caspase 3-mediated ablation, which led to a 54% reduction of  $\text{NST}^{\text{CART}}$  neurons, not only decreased baroreflex sensitivity but also reduced NREM sleep (Figures S4E–S4I).

We also tested the effect of optogenetic activation of  $\text{NST}^{\text{PE-TRAP}}$  and  $\text{NST}^{\text{CART}}$  neurons expressing ChR2 (Figures 4A, S3A, and S4A). Laser stimulation (constant light, 2 min/trial, applied randomly every 8–21 min) caused a rapid increase in NREM sleep in addition to decreases in blood pressure and heart rate (Figures 4B–4F, S3F, and S4C), consistent with the effects of chemogenetic activation. The effects of laser stimulation on blood pressure, heart rate, and NREM sleep were significantly correlated with the number of activated  $\text{NST}$  neurons measured by Fos immunohistochemistry, and the increase in NREM sleep was significantly correlated with the decreases in blood pressure and heart rate (Figure 4G), supporting the idea

**Figure 2.  $\text{NST}^{\text{PE-TRAP}}$  and  $\text{NST}^{\text{CART}}$  neurons are barosensitive**

- (A) Optrode recording from  $\text{NST}^{\text{PE-TRAP}}$  neurons in freely moving TRAP2 mice injected with AAV-DIO-ChR2-eYFP in NST. Left: experimental schematic. Middle: an example of simultaneously recorded blood pressure (BP, scale bars, 50 mmHg), ECG, spontaneous and laser-evoked  $\text{NST}$  spiking (scale bars, 100 ms, 0.5 mV). Blue dots, laser pulses. Right: comparison of laser-evoked (blue) and averaged spontaneous (red) spike waveforms and spike raster showing multiple laser stimulation trials at 15 and 30 Hz.
- (B) Firing rate (FR) of an example  $\text{NST}^{\text{PE-TRAP}}$  neuron (bottom) together with BP and heart rate (HR).
- (C) Scatter plot (top) and histogram distribution (bottom) of correlation coefficient (CC) between FR and BP for identified  $\text{NST}^{\text{PE-TRAP}}$  (blue),  $\text{NST}^{\text{CART}}$  (magenta), and unidentified (gray)  $\text{NST}$  neurons, computed with 5-s bin. Each point represents one neuron.
- (D) Time-lock of spiking activity to the heartbeat. Left: BP, ECG, and spike train of an example  $\text{NST}^{\text{PE-TRAP}}$  neuron. Right: cross-covariance between FR and HR (blue). Gray lines represent confidence intervals of time-shifted control after Bonferroni correction (see STAR Methods). Cells with at least one time point beyond the confidence intervals were considered significantly time locked.
- (E) BP (black) and FR (blue) of  $\text{NST}^{\text{PE-TRAP}}$  neurons before and after PE injection (0.5 mg/kg). The FR of each neuron was Z scored before being averaged across neurons ( $n = 15$ ). Time 0 indicates time of injection. Shading,  $\pm$  SEM.
- (F) Response of  $\text{NST}^{\text{CART}}$  neurons to saline or PE injection measured with calcium imaging. Top left: schematic showing fiber photometry imaging of  $\text{NST}^{\text{CART}}$  neuron activity in freely moving Cartpt-Cre mice injected with AAV-DIO-GCaMP6s, with simultaneous ECG and blood pressure recordings. Bottom left: fluorescence image showing GCaMP6s expression in the NST (black box in coronal diagram). Scale bars, 200  $\mu\text{m}$ . Middle: an example of simultaneously recorded calcium signals (top), BP (middle), and HR (bottom) following PE injection (dashed lines and arrowheads). Right: BP (black) and calcium signals of  $\text{NST}^{\text{CART}}$  neurons (magenta), before and after intravenous saline or PE injection (1 mg/mL, 10  $\mu\text{L}$ );  $n = 15$  trials from 4 mice. Shading,  $\pm$  SEM.
- (G) Monosynaptic inputs to  $\text{NST}^{\text{PE-TRAP}}$  and  $\text{NST}^{\text{CART}}$  neurons in the brain and the nodose ganglion (NG) revealed by rabies-mediated retrograde tracing. Left, schematic for rabies tracing from  $\text{NST}^{\text{PE-TRAP}}$  and  $\text{NST}^{\text{CART}}$  neurons. Middle, percentage of input neurons in the 10 main brain regions and the nodose ganglion. HPF, hippocampal formation; CTXsp, cortical subplate; STR, striatum; PAL, pallidum; TH, thalamus; HY, hypothalamus; MB, midbrain; P, pons; MY, medulla. Right, fluorescence images showing presynaptic cells in the nodose ganglion, with triple FISH of *mCherry*, *Piezo1*, and *Piezo2*. White arrowheads indicate *mCherry* and *Piezo1* co-labeled neurons. Yellow arrowheads indicate *mCherry* and *Piezo2* co-labeled neurons. Blue, DAPI. Scale bars, 50  $\mu\text{m}$ . Inset, percentage of *mCherry* neurons co-labeled by *Piezo1*, *Piezo2*, or *Piezo1* and 2 in the nodose ganglion. Error bars,  $\pm$ SEM.



(legend on next page)

that the somnogenic and cardiovascular effects are mediated by shared neurons. Notably, however, the decreases in blood pressure and heart rate were observed within seconds of laser onset in each brain state (Figure 4H), suggesting that the effect of  $\text{NST}^{\text{PE-TRAP}}$  neuron activation on cardiovascular activity—the primary function of these neurons—can occur even before a change in brain state. Contrary to the effect of activation, optogenetic inactivation of  $\text{NST}^{\text{PE-TRAP}}$  or  $\text{NST}^{\text{CART}}$  neurons through the inhibitory opsin iC++ (Berndt et al., 2016) caused a decrease in NREM sleep and increase in wakefulness (Figures 4D, 4F, S3D, S3F, and S4J), suggesting that the endogenous activity of these neurons also contributes to sleep regulation. In control mice expressing eYFP without ChR2 or iC++ in  $\text{NST}^{\text{PE-TRAP}}$  or  $\text{NST}^{\text{CART}}$  neurons, laser stimulation had no effect ( $\text{NST}^{\text{PE-TRAP}}$ : Figure S3E; NREM,  $p = 0.39$ ; wake,  $p = 0.20$ ; REM,  $p = 0.22$ , bootstrap;  $\text{NST}^{\text{CART}}$ : Figure S4B; NREM,  $p = 0.38$ ; wake,  $p = 0.41$ ; REM,  $p = 0.40$ ), and the laser-induced changes in brain states were significantly different between ChR2 and eYFP and between iC++ and eYFP mice (Figures 4D and 4F). Optogenetic activation of  $\text{NST}^{\text{Sal-TRAP}}$  neurons also had no significant effect (Figure S3G).

In contrast to  $\text{NST}^{\text{CART}}$  and  $\text{NST}^{\text{PE-TRAP}}$  neurons, which project strongly to the Amb and CLVM (Figures S5A, S5B, S7A, and S7B), tachykinin 1 (TAC1)-expressing NST neurons (largely non-overlapping with PE-TRAP neurons, Figure 1E) project strongly to the parabrachial nucleus (Figure S4K), known to contain wake-promoting neurons (Kaur et al., 2013). Optogenetic activation of TAC1 neurons promoted wakefulness (Figure S4L), indicating functional heterogeneity of NST neurons in sleep-wake regulation.

### Bidirectional manipulation of the vasomotor pathway

A major projection target of the NST is the CVLM, which contains GABAergic neurons that mediate baroreflex by inhibiting sympathoexcitatory neurons in the RVLM (Figures S5A, S5B, and S5E) (Dampney, 2016; Guyenet, 2006). Rabies-mediated retrograde tracing (Miyamichi et al., 2011; Wickersham et al., 2007) from the CVLM region of Gad2-Cre mice confirmed monosynaptic input from  $\text{NST}^{\text{CART}}$  neurons (Figures 5A and S5C). We next examined the function of this pathway in brain state regulation.

Optogenetic activation of GABAergic neurons in the CVLM region of Gad2-Cre mice caused a strong increase in NREM sleep ( $p < 0.0001$ , bootstrap, Figures 5B, 5F, and S6D) in addition to decreases in blood pressure and heart rate (Figure S6E). To test the contribution of RVLM neurons, we injected Cre-inducible

AAV expressing the inhibitory opsin iC++ into the RVLM of tyrosine hydroxylase (Th)-Cre mice (Figure S5D). Laser-induced inactivation of these RVLM neurons indeed caused a significant increase in NREM sleep ( $p < 0.0001$ , bootstrap, Figures 5C and 5G), suggesting that the effect of CVLM activation is at least partly mediated by inhibiting the RVLM adrenergic neurons, which are active during wakefulness (Figures S6A–S6C) and project to wake-promoting regions such as the locus coeruleus (Abbott et al., 2012) (Figure S5F). In contrast, iC++-mediated inactivation of CVLM GABAergic neurons caused a strong decrease in sleep ( $p < 0.0001$ , bootstrap, Figure 5D). This is likely mediated in part by disinhibition of the RVLM neurons, whose optogenetic activation promoted wakefulness (Abbott et al., 2013; Stornetta and Guyenet, 2018) ( $p < 0.0001$ , bootstrap, Figure 5E). In control mice expressing eYFP alone in the CVLM or RVLM, laser stimulation had no effect (CVLM: NREM,  $p = 0.34$ ; wake,  $p = 0.43$ ; REM,  $p = 0.10$ ; RVLM: NREM,  $p = 0.32$ ; wake,  $p = 0.36$ ; REM,  $p = 0.07$ , bootstrap), and the laser-induced changes were significantly different between ChR2 and control and between iC++ and control mice (Figures 5F, 5G, S6F, and S6G). Note, however, that the GABAergic neurons optogenetically manipulated in these experiments are likely to be functionally heterogeneous; some of them may be involved in other functions such as respiratory control, which in turn interacts with cardiovascular regulation (Benarroch, 2018; Dampney, 2016; Guyenet, 2006; Mandel and Schreiber, 2006). Our observations show that the GABAergic neurons in the CVLM region, previously associated mainly with autonomic control, also contribute strongly to the regulation of sleep-wake brain states.

### Cholinergic nucleus ambiguus promotes NREM sleep

Besides the CVLM, NST barosensitive neurons also project to the Amb, which contains parasympathetic cholinergic neurons mediating the cardiac component of baroreflex (Figures S7A and S7B) (Dampney, 2016; Guyenet, 2006). Rabies-mediated retrograde tracing from the Amb in ChAT-Cre mice confirmed monosynaptic input from  $\text{NST}^{\text{CART}}$  neurons (Figures 6A, S7C, and S7D). Because the long and thin shape of the Amb makes it difficult to activate a large fraction of the neurons optogenetically, we tested the effect of chemogenetic activation. In ChAT-Cre mice expressing hM3D(Gq)-mCherry in the Amb (Figures 6B and S7E), CNO injection caused a strong increase in NREM sleep in addition to a decrease in blood pressure and heart rate (Figure 6C). In control mice expressing mCherry without hM3D(Gq), CNO had no effect (Figure S7F), and the

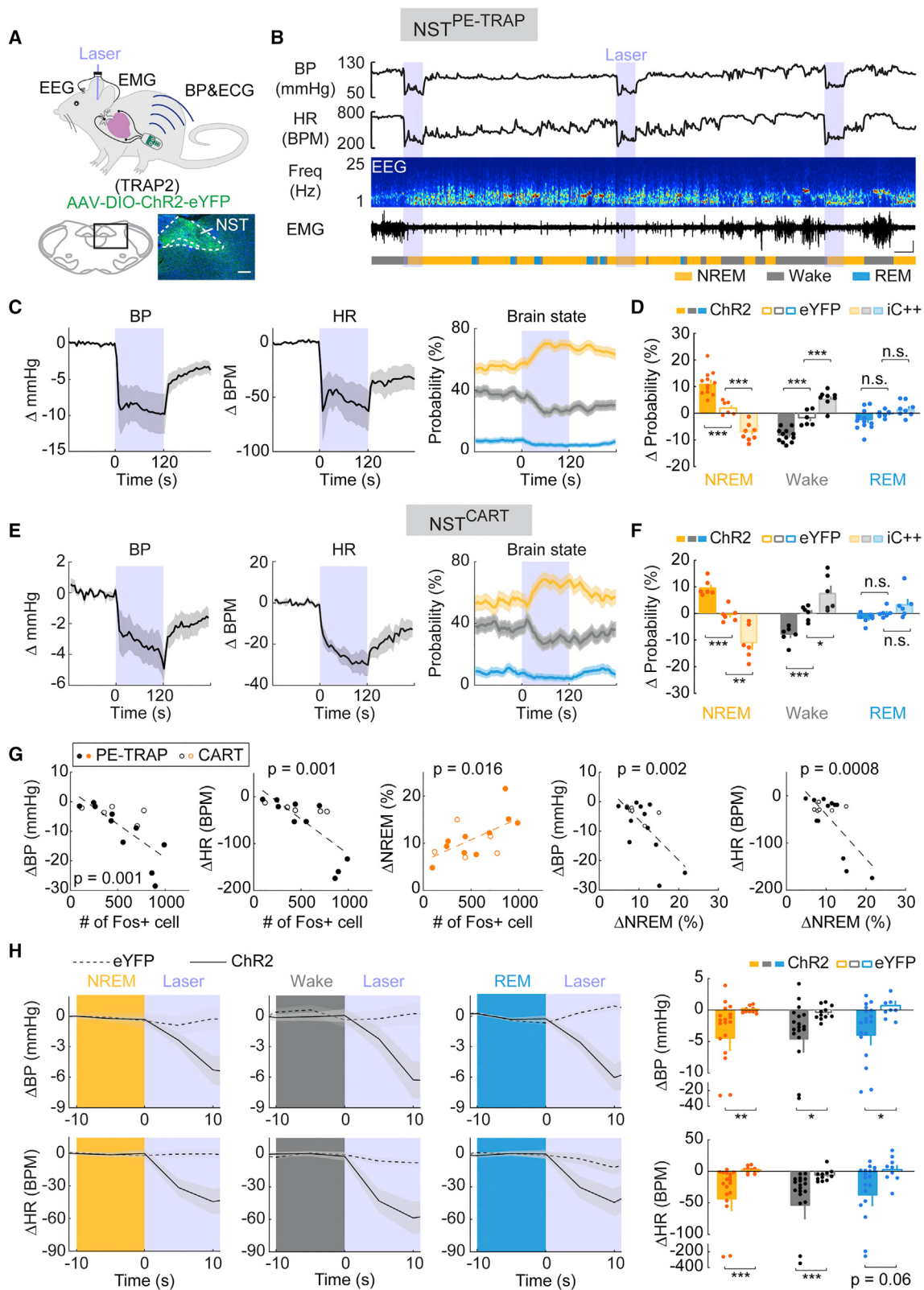
**Figure 3. Chemogenetic activation of  $\text{NST}^{\text{PE-TRAP}}$  or  $\text{NST}^{\text{CART}}$  neurons promotes NREM sleep**

(A) Schematic showing chemogenetic activation of  $\text{NST}^{\text{PE-TRAP}}$  neurons in freely moving TRAP2 mice injected with AAV-DIO-Gq-mCherry, with simultaneous EEG, EMG, ECG, and blood pressure recordings. Bottom: fluorescence image showing Gq-mCherry expression in the NST (black box in coronal diagram). Scale bars, 200  $\mu\text{m}$ .

(B) An example experiment. Shown are blood pressure (BP), heart rate (HR), EEG spectrogram, EMG trace (scale bars, 10 min, 1 mV), and brain states (color coded) with CNO or vehicle injection. BPM, beats per minute; Freq., frequency.

(C) Top: changes in BP and HR and probability (percentage of time) in NREM, wake, or REM state following CNO or vehicle injection (at time 0) in mice expressing hM3D(Gq). Horizontal axis, time after CNO/vehicle injection. \* $p < 0.05$ , \*\* $p < 0.01$ , \*\*\* $p < 0.001$  (two-way ANOVA with Bonferroni correction,  $n = 11$  mice). Error bar,  $\pm\text{SEM}$ . Bottom: CNO-induced changes in BP, HR, and each brain state (difference between CNO and saline averaged 0–3 h after injection) in mice expressing Gq or mCherry only. Each dot represents one mouse; error bars,  $\pm\text{SEM}$ .  $p = 0.0010$  (BP, t test), 0.0011 (HR, Mann-Whitney U test),  $<0.0001$  (NREM, t test),  $<0.0001$  (wake, t test), 0.05 (REM, t test). \*\* $p < 0.01$ , \*\*\* $p < 0.001$ .

(D) Similar to (C), for chemogenetic activation of  $\text{NST}^{\text{CART}}$  neurons ( $n = 6$  mice per group).  $p = 0.014$  (BP), 0.0063 (HR), 0.0043 (NREM), 0.0011 (wake), 0.33 (REM), t test.



(legend on next page)

CNO-induced change in brain state was significantly different between hM3D(Gq) and control mice (Figure 6C). Because the Amb contains cholinergic neurons innervating the esophagus and bronchus in addition to the heart, the sleep-promoting effect could be mediated by a larger parasympathetic population than those specific for baroreflex.

## DISCUSSION

In this study, we used activity-dependent genetic labeling (Allen et al., 2017; Guenthner et al., 2013) to tag NST neurons activated by PE-induced blood pressure elevation (Figure 1). Optrode recording and calcium imaging confirmed barosensitivity of the tagged neurons on subsecond to second timescales (Figure 2). Chemogenetic or optogenetic activation of these neurons promoted NREM sleep in addition to decreasing the blood pressure and heart rate (Figures 3 and 4). Bidirectional manipulation of CVLM GABAergic neurons demonstrated their significant contribution to sleep-wake regulation, at least in part mediated by the inhibition of RVLM adrenergic neurons, which are wake active and wake promoting as well as sympathoexcitatory (Abbott et al., 2012; Bochorishvili et al., 2014; Stornetta and Guyenet, 2018) (Figure 5). In addition to the CVLM → RVLM vasomotor pathway, activating the Amb cardiac pathway promoted NREM sleep as well (Figure 6). A previous study showed that hypothalamic neurons that are activated by warm temperatures can cause both a decrease in body temperature and increase in NREM sleep (Harding et al., 2018), indicating a shared mechanism for autonomic and sleep control. Our results show that neurons in the lower brain stem responsible for a basic cardiovascular reflex are also part of the sleep regulation mechanism.

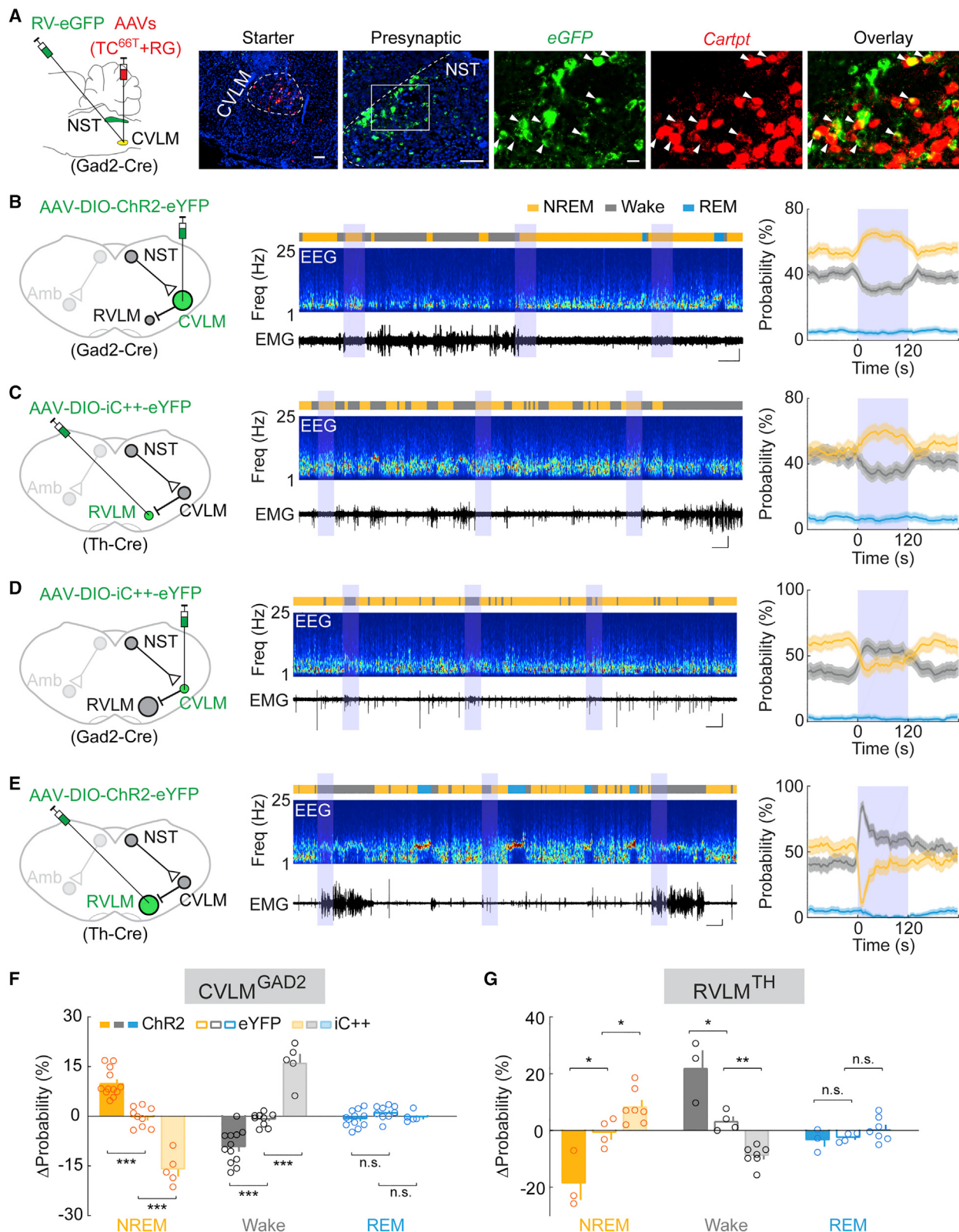
Previous recording, lesion, electrical stimulation, and pharmacological manipulation experiments have shown that the NST contributes to sleep-like EEG synchronization (Batinis et al., 1958; Cordeau and Mancia, 1959; Eguchi and Satoh, 1980; Laguzzi et al., 1984; Magnes et al., 1961). Here, we show that although some NST neurons can promote wakefulness (Figure S4L), the subset activated by blood pressure elevation promote NREM sleep in addition to decreasing cardiovascular output (Figures 3 and 4), providing a cell-type-specific circuit

mechanism coordinating the regulation of brain state and autonomic motor activity (Liu and Dan, 2019). Because the firing rates of  $\text{NST}^{\text{PE-TRAP}}$  neurons increase with the blood pressure (Figures 2B and 2C), on average they are higher during wakefulness than sleep (Wake,  $15.8 \pm 3.2$ ; NREM,  $11.4 \pm 2.8$ ; REM,  $10.8 \pm 2.2$  spikes/s); optogenetic activation of these neurons can also cause rapid decreases in blood pressure and heart rate before any change in sleep-wake brain states (Figure 4H). Thus, unlike the typical “sleep neurons” found in other brain regions that are mainly involved in sleep regulation (Scammell et al., 2017; Zhang et al., 2019; Zhong et al., 2019), the  $\text{NST}^{\text{PE-TRAP}}$  neurons engage primarily in cardiovascular control and only “moonlight” in sleep regulation as a secondary function. We note that the  $\text{NST}^{\text{PE-TRAP}}$  and  $\text{NST}^{\text{CART}}$  populations only overlap partially (Figures 1E and S1B), and it would be important for future studies to identify better genetic markers for NST barosensitive neurons.

The sleep-promoting effect is partly mediated by the  $\text{NST} \rightarrow \text{CVLM} \rightarrow \text{RVLM}$  pathway for vasomotor baroreflex (Figure 5). Adrenergic neurons in the RVLM are known to provide excitatory projections to multiple wake-promoting populations, including noradrenergic neurons in the locus coeruleus (Abbott et al., 2012) and orexinergic neurons in the hypothalamus (Bochorishvili et al., 2014). Activation of NST barosensitive neurons and CVLM GABAergic neurons should cause inhibition of RVLM neurons, thus reducing the excitation of their downstream wake-promoting neurons. In addition, previous studies showed that an acute increase in blood pressure can promote arousal (Fewell and Johnson, 1984; Kesler et al., 1999), likely through mechanisms separate from the baroreflex circuit (e.g., a blood pressure increase could change the cerebral blood volume and oxygen level (Meng et al., 2012), which could in turn affect neuronal activity). Aside from reducing excitation of the wake-promotion neurons innervated by RVLM, activation of the vasomotor baroreflex pathway could also decrease arousal through the lowering of blood pressure. Activity of the cholinergic Amb is known to reduce cardiac output through its projection to the heart (Dampney, 2016; Guyenet, 2006). How its activation promotes NREM sleep (Figure 6) remains to be investigated. Furthermore, both the Amb cholinergic and CVLM GABAergic neurons are

**Figure 4. Optogenetic activation of  $\text{NST}^{\text{PE-TRAP}}$  or  $\text{NST}^{\text{CART}}$  neurons promotes NREM sleep**

- (A) Schematic showing optogenetic activation of  $\text{NST}^{\text{PE-TRAP}}$  neurons in freely moving TRAP2 mice injected with AAV-DIO-ChR2-eYFP, with simultaneous EEG, EMG, ECG, and blood pressure (BP) recordings. Bottom: fluorescence image showing ChR2-eYFP expression in the NST (black box in coronal diagram). Scale bars, 200  $\mu\text{m}$ .
- (B) An example experiment with optogenetic activation of  $\text{NST}^{\text{PE-TRAP}}$  neurons. Shown are BP, heart rate (HR), EEG spectrogram, EMG trace, and brain states (color coded). Blue stripe, laser stimulation period (constant light, 120 s). BPM, beats per minute; Freq., frequency.
- (C) Changes in BP and HR and percentage of time in NREM, REM, or wake state before, during, and after laser stimulation in mice expressing ChR2-eYFP in  $\text{NST}^{\text{TRAP}}$  neurons ( $n = 12$  mice). Shading for BP and HR,  $\pm\text{SEM}$ ; shading for Brain state, 95% confidence intervals. Blue strip, laser stimulation period.
- (D) Laser-induced changes in each state in mice expressing ChR2-eYFP, eYFP only, or iC++-eYFP. Each dot represents one mouse. Error bars,  $\pm\text{SEM}$ . n.s., not significant, \*\*\* $p < 0.001$  (t test); ChR2 versus eYFP:  $p = 0.0003$  (NREM),  $= 0.0001$  (wake),  $= 0.18$  (REM); eYFP versus iC++:  $p < 0.0001$  (NREM),  $= 0.0006$  (wake),  $= 0.16$  (REM).
- (E) and (F) Similar to (C and D) for optogenetic activation of  $\text{NST}^{\text{CART}}$  neurons ( $n = 6$  mice per group); ChR2 versus eYFP:  $p = 0.0008$  (NREM),  $= 0.0001$  (wake),  $= 0.097$  (REM); eYFP versus iC++:  $p = 0.0039$  (NREM),  $= 0.03$  (wake),  $= 0.20$  (REM).
- (G) Changes in BP, HR, and NREM versus number of Fos+ cells, and laser-induced changes in BP and HR versus change in NREM sleep. Dashed lines indicate linear regression.
- (H) Laser-induced changes in BP and HR in mice expressing ChR2-eYFP (12 PE-TRAP, 6 Cartpt-Cre mice) or eYFP only (6 PE-TRAP, 5 Cartpt-Cre mice) within each brain state. For comparison between the ChR2 and eYFP groups, NREM:  $p = 0.007$  (BP),  $< 0.0001$  (HR); wake:  $p = 0.018$  (BP),  $0.0009$  (HR); REM:  $p = 0.020$  (BP),  $0.06$  (HR), Mann-Whitney U test. \* $p < 0.05$ , \*\* $p < 0.01$ , \*\*\* $p < 0.001$ . Error bars,  $\pm\text{SEM}$ .



(legend on next page)

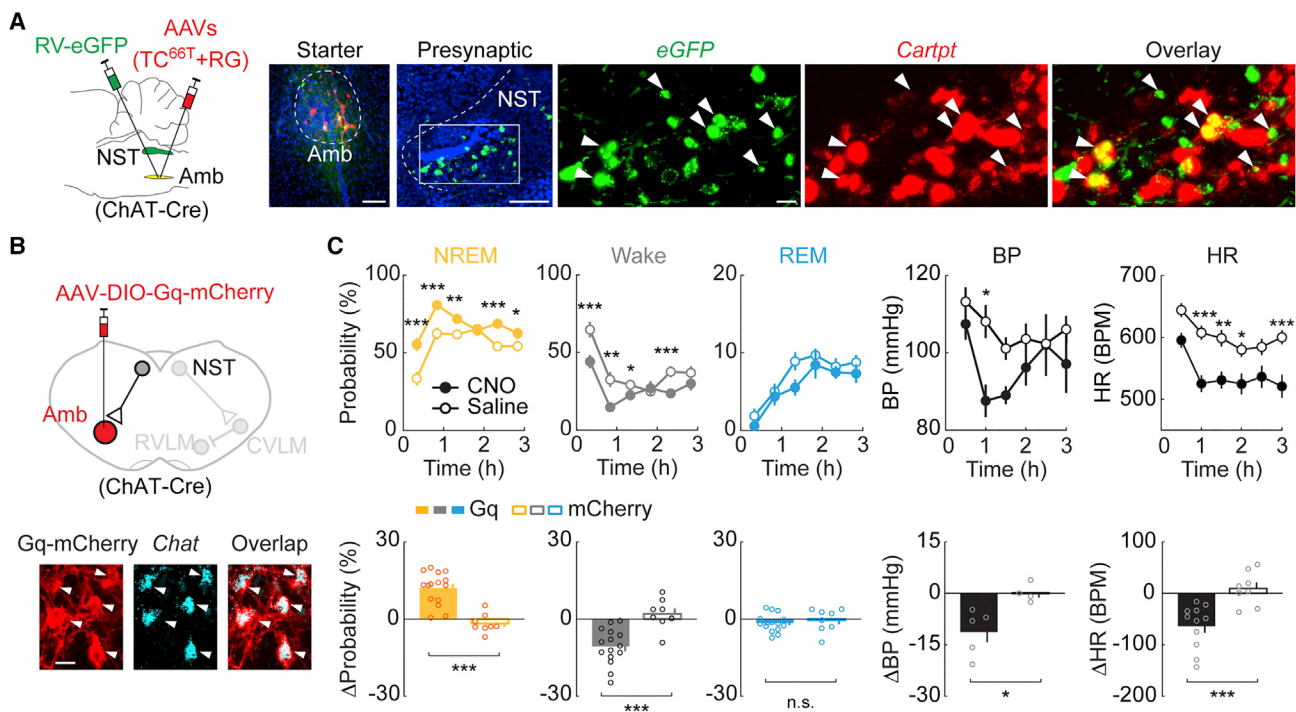


**Figure 6. Activity of NST → Amb pathway promotes sleep**

(A) Monosynaptic innervation of Amb cholinergic neuron by NST<sup>CART</sup> neurons. Fluorescence images show starter and presynaptic cells in rabies-mediated tracing. Blue, DAPI. Scale bars, 100 µm. Double FISH of eGFP and *Cartpt* in the region in white box are shown on the right. Arrowheads indicate co-labeled neurons. Scale bars, 20 µm.

(B) Top: schematic with NST → Amb circuit depicted on the left side of coronal diagram. Circle size represents expected activation of the neuronal population. Bottom: fluorescence images showing co-localization of Gq-mCherry and *Chat*. Scale bars, 20 µm.

(C) Effects of chemogenetic activation of Amb cholinergic neurons. Top: percentage of time in each brain state and BP, HR following CNO or saline injection in mice expressing hM3D(Gq). Horizontal axis, time after CNO/vehicle injection. Error bar, ±SEM. \* p < 0.05, \*\* p < 0.01, \*\*\* p < 0.001 (two-way ANOVA with Bonferroni correction). Bottom: CNO-induced changes in each brain state, BP, and HR (difference between CNO and vehicle averaged 0–3 h after injection) in mice expressing Gq or mCherry only. Each dot represents one mouse. \*p < 0.05, \*\*p < 0.001 (t test); p < 0.0001 (NREM), = 0.0003 (wake), 0.053 (REM), 0.016 (BP), and 0.0009 (HR).

functionally diverse; only a subset of them is responsible for cardiovascular control (Stornetta et al., 2013). In future studies it would be of great interest to test the contribution of the cardiovascular subset in sleep regulation, especially in conjunction with the manipulation of NST barosensitive neurons. In addition to the CVLM and Amb, NST neurons also project to other brain

regions, such as the hypothalamus (Dampney, 2016; Guyenet, 2006), which could contribute to their sleep-promoting effect as well.

Physical stimulation of baroreceptors has been shown to induce sleep-like states (Bonvallet et al., 1954; Bridgers et al., 1985; Dell and Padel, 1965; Dell and Marillau, 1966;

**Figure 5. Activity of NST → CVLM → RVLM pathway regulates sleep**

(A) Monosynaptic innervation of CVLM GABAergic neurons by NST<sup>CART</sup> neurons. Fluorescence images show starter and presynaptic cells in rabies-mediated tracing. Blue, DAPI. Scale bars, 100 µm. Double FISH of eGFP and *Cartpt* in the region in white box are shown on the right. Arrowheads indicate co-labeled neurons. Scale bars, 20 µm.

(B) Optogenetic activation of CVLM GABAergic neurons promotes NREM sleep. Left: schematic with NST → CVLM → RVLM circuit depicted on the right side of coronal diagram.  $\rightarrow$ , excitatory;  $\rightarrow$ , inhibitory. Circle size represents expected degree of activation of the neuronal population (e.g., activation of CVLM neurons is expected to inhibit RVLM neurons). Middle: an example optogenetic activation experiment in Gad2-Cre mouse with AAV-DIO-ChR2-eYFP injected into CVLM. Shown are EEG spectrogram, EMG trace, and brain states (color coded). Blue stripe, laser stimulation period (constant light, 120 s). Freq., frequency. Right: percentage of time in NREM, REM, or wake state before, during, and after laser stimulation (n = 12 mice). Shading, 95% confidence intervals.

(C-E) Similar to (B), for optogenetic inactivation of RVLM (C, n = 7 mice), inactivation of CVLM (D, n = 5 mice), and activation of RVLM (E, n = 3 mice). Scale bars under EMG traces, 120 s, 1 mV.

(F) Laser-induced changes in each state in mice expressing ChR2-eYFP, eYFP only, or iC++-eYFP in CVLM of Gad2-Cre mice. Each point represents one mouse. n.s., not significant, \*\*\*p < 0.001 (t test); ChR2 versus eYFP: p < 0.0001 (NREM), = 0.0002 (wake), 0.07 (REM); eYFP versus iC++: p < 0.0001 (NREM), < 0.0001 (wake), = 0.24 (REM). Error bars, ±SEM.

(G) Similar to (F), for mice expressing ChR2-eYFP, eYFP only, or iC++-eYFP in RVLM of Th-Cre mice. \*p < 0.05, \*\*p < 0.01; ChR2 versus eYFP: p = 0.026 (NREM), 0.021 (wake), 0.70 (REM); eYFP versus iC++: p = 0.031 (NREM), 0.0011 (wake), 0.24 (REM).

Koch, 1932; Mazzella et al., 1957; Padel and Dell, 1965), but these early reports have been partially forgotten and the effects are thought to be limited to anesthetized conditions (Silvani et al., 2015). In addition, the circuit mechanism mediating the effect of baroreceptor stimulation on brain states was unknown. Here, we have shown, in freely moving mice, that optogenetic or chemogenetic activation of each stage of the baroreflex pathway strongly promotes sleep. In humans, baroreceptors are more activated in the supine than the upright position, which could cause higher activation of the baroreflex pathway and thus promote sleep (Cole, 1989). Our findings suggest that the artificial activation of baroreceptors, which can be achieved through noninvasive techniques (Cooper and Hainsworth, 2009), may provide an effective solution for sleep enhancement.

## STAR★METHODS

Detailed methods are provided in the online version of this paper and include the following:

- **KEY RESOURCES TABLE**
- **RESOURCE AVAILABILITY**
  - Lead contact
  - Materials availability
  - Data and code availability
- **EXPERIMENTAL MODEL AND SUBJECT DETAILS**
- **METHOD DETAILS**
  - Virus preparation
  - Surgical procedures
  - TRAP induction
  - BP and ECG recordings
  - Optrode recording
  - Polysomnographic recordings
  - Optogenetic manipulation
  - Chemogenetic manipulation
  - Fiber photometry recording and analysis
  - Immunohistochemistry and fluorescence *in situ* hybridization (FISH)
  - Whole-brain anatomical quantification
- **QUANTIFICATION AND STATISTICAL ANALYSIS**

## SUPPLEMENTAL INFORMATION

Supplemental information can be found online at <https://doi.org/10.1016/j.neuron.2022.08.027>.

## ACKNOWLEDGMENTS

We thank F. Weber for help with optrode recording analysis, University of North Carolina Virus Core, Salk Institute Virus Core for supplying AAVs, and LifeCanvas Technologies for whole-brain mapping of PE-Fos and PE-TRAP signals. This work was supported by HHMI and Nan Fung Life Sciences Chancellor's Chair fund.

## AUTHOR CONTRIBUTIONS

Y.Y. and Y.D. conceived and designed the study and wrote the paper; Y.Y. performed most of the experiments; Z.B., D.D., D.S., and D.L. wrote programs for data analysis; Y.Y., Z.B., and D.D. analyzed the data; C.F.T. and Y.Y. performed TRAP induction; D.S. and Y.Y. performed fiber photometry recording and analyzed data; C.M., A.C., S.Y., and H.Z. provided virus for RV tracing;

M.S.D. performed some histology and FISH experiments. Y.D. supervised all aspects of the work.

## DECLARATION OF INTERESTS

Y.D. and H.Z. are members of the advisory board for the journal *Neuron*.

Received: April 4, 2022

Revised: July 2, 2022

Accepted: August 29, 2022

Published: September 27, 2022

## REFERENCES

- Abbott, S.B., Coates, M.B., Stornetta, R.L., and Guyenet, P.G. (2013). Optogenetic stimulation of c1 and retrotrapezoid nucleus neurons causes sleep state-dependent cardiorespiratory stimulation and arousal in rats. *Hypertension* 61, 835–841.
- Abbott, S.B., Kanbar, R., Bochorishvili, G., Coates, M.B., Stornetta, R.L., and Guyenet, P.G. (2012). C1 neurons excite locus coeruleus and A5 noradrenergic neurons along with sympathetic outflow in rats. *J. Physiol.* 590, 2897–2915.
- Allen, W.E., DeNardo, L.A., Chen, M.Z., Liu, C.D., Loh, K.M., Fennel, L.E., Ramakrishnan, C., Deisseroth, K., and Luo, L. (2017). Thirst-associated preoptic neurons encode an aversive motivational drive. *Science* 357, 1149–1155.
- Anikeeva, P., Andelman, A.S., Witten, I., Warden, M., Goshen, I., Grosenick, L., Gunaydin, L.A., Frank, L.M., and Deisseroth, K. (2011). Optetrode: a multi-channel readout for optogenetic control in freely moving mice. *Nat. Neurosci.* 15, 163–170.
- Balan Júnior, A., Caous, C.A., Yu, Y.G., and Lindsey, C.J. (2004). Barosensitive neurons in the rat tractus solitarius and paratrigeminal nucleus: a new model for medullary, cardiovascular reflex regulation. *Can. J. Physiol. Pharmacol.* 82, 474–484.
- Batini, C., Moruzzi, G., Palestini, M., Rossi, G.F., and Zanchetti, A. (1958). Persistent patterns of wakefulness in the pretrigeminal midpontine preparation. *Science* 128, 30–32.
- Benarroch, E.E. (2018). Brainstem integration of arousal, sleep, cardiovascular, and respiratory control. *Neurology* 91, 958–966.
- Berg, S., Kutra, D., Kroeger, T., Straehle, C.N., Kausler, B.X., Haubold, C., Schiegg, M., Ales, J., Beier, T., Rudy, M., et al. (2019). ilastik: interactive machine learning for (bio)image analysis. *Nat. Methods* 16, 1226–1232.
- Berndt, A., Lee, S.Y., Wietek, J., Ramakrishnan, C., Steinberg, E.E., Rashid, A.J., Kim, H., Park, S., Santoro, A., Frankland, P.W., et al. (2016). Structural foundations of optogenetics: determinants of channelrhodopsin ion selectivity. *Proc. Natl. Acad. Sci. USA* 113, 822–829.
- Bochorishvili, G., Nguyen, T., Coates, M.B., Viar, K.E., Stornetta, R.L., and Guyenet, P.G. (2014). The orexinergic neurons receive synaptic input from C1 cells in rats. *J. Comp. Neurol.* 522, 3834–3846.
- Bonvallet, M., Dell, P., and Hiebel, G. (1954). Tonus sympathique et activité électrique corticale. *Electroencephalogr. Clin. Neurophysiol.* 6, 119–144.
- Bridgers, S.L., Spencer, S.S., Spencer, D.D., and Sasaki, C.T. (1985). A cerebral effect of carotid sinus stimulation. Observation during intraoperative electroencephalographic monitoring. *Arch. Neurol.* 42, 574–577.
- Chan, R.K., and Sawchenko, P.E. (1998). Organization and transmitter specificity of medullary neurons activated by sustained hypertension: implications for understanding baroreceptor reflex circuitry. *J. Neurosci.* 18, 371–387.
- Chen, T.W., Wardill, T.J., Sun, Y., Pulver, S.R., Renninger, S.L., Baohan, A., Schreiter, E.R., Kerr, R.A., Orger, M.B., Jayaraman, V., et al. (2013). Ultrasensitive fluorescent proteins for imaging neuronal activity. *Nature* 499, 295–300.
- Cole, R.J. (1989). Postural baroreflex stimuli may affect EEG arousal and sleep in humans. *J. Appl. Physiol.* (1985) 67, 2369–2375.
- Conway, J., Boon, N., Jones, J.V., and Sleight, P. (1983). Involvement of the baroreceptor reflexes in the changes in blood pressure with sleep and mental arousal. *Hypertension* 5, 746–748.

- Cooper, V.L., and Hainsworth, R. (2009). Carotid baroreflex testing using the neck collar device. *Clin. Auton. Res.* 19, 102–112.
- Cordeau, J.P., and Mancia, M. (1959). Evidence for the existence of an electroencephalographic synchronization mechanism originating in the lower brain stem. *Electroencephalogr. Clin. Neurophysiol.* 11, 551–564.
- Dampney, R.A. (2016). Central neural control of the cardiovascular system: current perspectives. *Adv. Physiol. Educ.* 40, 283–296.
- Dampney, R.A., Polson, J.W., Potts, P.D., Hirooka, Y., and Horiuchi, J. (2003). Functional organization of brain pathways subserving the baroreceptor reflex: studies in conscious animals using immediate early gene expression. *Cell. Mol. Neurobiol.* 23, 597–616.
- Dell, P., and Marillau, A. (1966). Nature des afférences et rôle de la région solitaire dans l'endormissement d'origine vago-aortique. *Rev. Neurol. Paris* 115, 161–162.
- Dell, P., and Padel, Y. (1965). Rapid falling asleep provoked by selective stimulation of vagal afferents in the cat. *Electroencephalogr. Clin. Neurophysiol.* 18, 725.
- Eguchi, K., and Satoh, T. (1980). Convergence of sleep-wakefulness subsystems onto single neurons in the region of cat's solitary tract nucleus. *Arch. Ital. Biol.* 118, 331–345.
- Fewell, J.E., and Johnson, P. (1984). Acute increases in blood pressure cause arousal from sleep in lambs. *Brain Res.* 311, 259–265.
- Groeneboom, N.E., Yates, S.C., Puchades, M.A., and Bjaalie, J.G. (2020). Nutil: a pre- and post-processing toolbox for histological rodent brain section images. *Front. Neuroinform.* 14, 37.
- Guenther, C.J., Miyamichi, K., Yang, H.H., Heller, H.C., and Luo, L. (2013). Permanent genetic access to transiently active neurons via TRAP: targeted recombination in active populations. *Neuron* 78, 773–784.
- Guyenet, P.G. (2006). The sympathetic control of blood pressure. *Nat. Rev. Neurosci.* 7, 335–346.
- Harding, E.C., Yu, X., Miao, A., Andrews, N., Ma, Y., Ye, Z., Lignos, L., Miracca, G., Ba, W., Yustos, R., et al. (2018). A neuronal hub binding sleep initiation and body cooling in response to a warm external stimulus. *Curr. Biol.* 28, e2263.e4–e2273.e4.
- Hauswirth, W.W., Lewin, A.S., Zolotukhin, S., and Muzyczka, N. (2000). Production and purification of recombinant adeno-associated virus. *Methods Enzymol.* 316, 743–761.
- Hayward, L.F., and Felder, R.B. (1995). Cardiac rhythmicity among NTS neurons and its relationship to sympathetic outflow in rabbits. *Am. J. Physiol.* 269, H923–H933.
- Kaur, S., Pedersen, N.P., Yokota, S., Hur, E.E., Fuller, P.M., Lazarus, M., Chamberlin, N.L., and Saper, C.B. (2013). Glutamatergic signaling from the parabrachial nucleus plays a critical role in hypercapnic arousal. *J. Neurosci.* 33, 7627–7640.
- Kesler, B., Anand, A., Launois, S.H., and Weiss, J.W. (1999). Drug-induced arterial pressure elevation is associated with arousal from NREM sleep in normal volunteers. *J. Appl. Physiol.* (1985) 87, 897–901.
- Kmiotek, E.K., Baimel, C., and Gill, K.J. (2012). Methods for intravenous self-administration in a mouse model. *J. Vis. Exp.* e3739.
- Koch, E. (1932). Die Irradiation der Pressorezeptorischen Kreislaufreflexe. *Klin. Wochenschr.* 11, 225–227.
- Krashes, M.J., Koda, S., Ye, C., Rogan, S.C., Adams, A.C., Cusher, D.S., Maratos-Flier, E., Roth, B.L., and Lowell, B.B. (2011). Rapid, reversible activation of AgRP neurons drives feeding behavior in mice. *J. Clin. Invest.* 121, 1424–1428.
- Laguzzi, R., Reis, D.J., and Talman, W.T. (1984). Modulation of cardiovascular and electrocortical activity through serotonergic mechanisms in the nucleus tractus solitarius of the rat. *Brain Res.* 304, 321–328.
- Lerner, T.N., Shilyansky, C., Davidson, T.J., Evans, K.E., Beier, K.T., Zalocousky, K.A., Crow, A.K., Malenka, R.C., Luo, L., Tomer, R., and Deisseroth, K. (2015). Intact-brain analyses reveal distinct information carried by SNC dopamine subcircuits. *Cell* 162, 635–647.
- Liu, D., and Dan, Y. (2019). A motor theory of sleep-wake control: arousal-action circuit. *Annu. Rev. Neurosci.* 42, 27–46.
- Magnes, J., Moruzzi, G., and Pompeiano, O. (1961). Synchronization of the EEG produced by low-frequency electrical stimulation of the region of the solitary tract. *Arch. Ital. Biol.* 99, 33–67.
- Mandel, D.A., and Schreihofner, A.M. (2006). Central respiratory modulation of barosensitive neurones in rat caudal ventrolateral medulla. *J. Physiol.* 572, 881–896.
- Mazzella, H., Garcia Mullin, R., and Garcia Aust, E. (1957). Effect of carotid sinus stimulation on the EEG. *Acta Neurol. Latinoam.* 3, 361–364.
- Meng, L., Gelb, A.W., Alexander, B.S., Cerussi, A.E., Tromberg, B.J., Yu, Z., and Mantulin, W.W. (2012). Impact of phenylephrine administration on cerebral tissue oxygen saturation and blood volume is modulated by carbon dioxide in anaesthetized patients. *Br. J. Anaesth.* 108, 815–822.
- Min, S., Chang, R.B., Prescott, S.L., Beeler, B., Joshi, N.R., Strochlic, D.E., and Liberles, S.D. (2019). Arterial baroreceptors sense blood pressure through decorated aortic claws. *Cell Rep.* 29, 2192.e3–2201.e3.
- Miyamichi, K., Amat, F., Moussavi, F., Wang, C., Wickersham, I., Wall, N.R., Taniguchi, H., Tasic, B., Huang, Z.J., He, Z., et al. (2011). Cortical representations of olfactory input by trans-synaptic tracing. *Nature* 472, 191–196.
- Osakada, F., and Callaway, E.M. (2013). Design and generation of recombinant rabies virus vectors. *Nat. Protoc.* 8, 1583–1601.
- Padel, Y., and Dell, P. (1965). Effets bulbares et réticulaires des stimulations endormantes du tronc vago-aortique. *J. Physiol. Paris* 57, 269–270.
- Puchades, M.A., Csucs, G., Ledergerber, D., Leergaard, T.B., and Bjaalie, J.G. (2019). Spatial registration of serial microscopical brain images to three-dimensional reference atlases with the QuickNII tool. *PLoS One* 14, e0216796.
- Rogers, R.F., Paton, J.F., and Schwaber, J.S. (1993). NTS neuronal responses to arterial pressure and pressure changes in the rat. *Am. J. Physiol.* 265, R1355–R1368.
- Scammell, T.E., Arrigoni, E., and Lipton, J.O. (2017). Neural circuitry of wakefulness and sleep. *Neuron* 93, 747–765.
- Silvani, A., Calandra-Buonaura, G., Benarroch, E.E., Dampney, R.A., and Cortelli, P. (2015). Bidirectional interactions between the baroreceptor reflex and arousal: an update. *Sleep Med.* 16, 210–216.
- Silvani, A., and Dampney, R.A. (2013). Central control of cardiovascular function during sleep. *Am. J. Physiol. Heart Circ. Physiol.* 305, H1683–H1692.
- Smyth, H.S., Sleight, P., and Pickering, G.W. (1969). Reflex regulation of arterial pressure during sleep in man. A quantitative method of assessing baroreflex sensitivity. *Circ. Res.* 24, 109–121.
- Somers, V.K., Dyken, M.E., Mark, A.L., and Abboud, F.M. (1993). Sympathetic-nerve activity during sleep in normal subjects. *N. Engl. J. Med.* 328, 303–307.
- Stornetta, R.L., and Guyenet, P.G. (2018). C1 neurons: a nodal point for stress? *Exp. Physiol.* 103, 332–336.
- Stornetta, R.L., Macon, C.J., Nguyen, T.M., Coates, M.B., and Guyenet, P.G. (2013). Cholinergic neurons in the mouse rostral ventrolateral medulla target sensory afferent areas. *Brain Struct. Funct.* 218, 455–475.
- Tang, X., and Dworkin, B.R. (2010). Baroreflexes of the rat. VI. Sleep and responses to aortic nerve stimulation in the dmNTS. *Am. J. Physiol. Regul. Integr. Comp. Physiol.* 298, R1428–R1434.
- Tobaldini, E., Costantino, G., Solbiati, M., Cogliati, C., Kara, T., Nobili, L., and Montano, N. (2017). Sleep, sleep deprivation, autonomic nervous system and cardiovascular diseases. *Neurosci. Biobehav. Rev.* 74, 321–329.
- Wickersham, I.R., Finke, S., Conzelmann, K.K., and Callaway, E.M. (2007). Retrograde neuronal tracing with a deletion-mutant rabies virus. *Nat. Methods* 4, 47–49.
- Yates, S.C., Groeneboom, N.E., Coello, C., Lichtenthaler, S.F., Kuhn, P.H., Demuth, H.U., Hartlage-Rübsamen, M., Roßner, S., Leergaard, T., Kreshuk, A., et al. (2019). QUINT: workflow for quantification and spatial analysis of features in histological images from rodent brain. *Front. Neuroinform.* 13, 75.

- Zeng, W.Z., Marshall, K.L., Min, S., Daou, I., Chapleau, M.W., Abboud, F.M., Liberles, S.D., and Patapoutian, A. (2018). PIEZOs mediate neuronal sensing of blood pressure and the baroreceptor reflex. *Science* **362**, 464–467.
- Zhang, Z., Zhong, P., Hu, F., Barger, Z., Ren, Y., Ding, X., Li, S., Weber, F., Chung, S., Palmiter, R.D., and Dan, Y. (2019). An excitatory circuit in the peri-oculomotor midbrain for non-REM sleep control. *Cell* **177**, 1293.e16–1307.e16.
- Zhong, P., Zhang, Z., Barger, Z., Ma, C., Liu, D., Ding, X., and Dan, Y. (2019). Control of non-REM sleep by midbrain neurotensinergic neurons. *Neuron* **104**, 795.e6–809.e6.

## STAR★METHODS

### KEY RESOURCES TABLE

REAGENT or RESOURCE	SOURCE	IDENTIFIER
<b>Antibodies</b>		
Chicken anti-GFP for immunochemistry	Aves Labs	GFP-1020; RRID: AB_10000240
Rat anti-mCherry for immunochemistry	Thermo Fisher Scientific	Cat# M11217; RRID: AB_2536611
Rabbit anti-cFos for immunochemistry	Synaptic System	Cat# 226003; RRID: AB_2231974
<b>Bacterial and virus strains</b>		
AAV2-EF1 $\alpha$ -DIO-ChR2-eYFP	UNC Chapel Hill Vector Core	N/A
AAV2-EF1 $\alpha$ -DIO-iC++-eYFP	UNC Chapel Hill Vector Core	N/A
AAV2-EF1 $\alpha$ -DIO-eYFP	UNC Chapel Hill Vector Core	N/A
AAV2-EF1 $\alpha$ -DIO-hM3D(Gq)-mCherry	UNC Chapel Hill Vector Core	N/A
AAV2-EF1 $\alpha$ -DIO-mCherry	UNC Chapel Hill Vector Core	N/A
AAV2-hSyn-DIO-hM3D(Gq)-mCherry	Krashes et al., 2011	Addgene viral prep # 44361-AAV2; RRID: Addgene_44361
AAV2-hSyn-DIO-mCherry	Addgene (from Bryan Roth)	Addgene viral prep # 50459-AAV2; RRID: Addgene_50459
AAV2-EF1 $\alpha$ -DIO-taCasp3-TEVp	UNC Chapel Hill Vector Core	N/A
AAV9-CAG-FLEX-GCaMP6s-WPRE.SV40	Chen et al., 2013	Addgene viral prep # 100842-AAV9; RRID: Addgene_100842
AAV8-hSyn-FLEX-TVA-P2A-eGFP-2A-oG	Gene Transfer, Targeting and Therapeutics Facility of Salk Institute	N/A
G-Deleted rabies-mCherry	Gene Transfer Targeting and Therapeutics Core of Salk Institute	N/A
AAV2-CAG-FLEX-TC66T	Gift from Liqian Luo lab, Stanford University	N/A
AAV2-CAG-FLEX-RG	Gift from Liqian Luo lab, Stanford University	N/A
CVS N2c dG Histone-eGFP (H2BeGFP)	from A. Cetin and H. Zeng in the Allen Institute for Brain Science	N/A
<b>Chemicals, peptides, and recombinant proteins</b>		
Clozapine-N-oxide	Sigma-Aldrich	C0832
Phenylephrine	Sigma-Aldrich	P1240000
4-hydroxytamoxifen	Sigma-Aldrich	H6278
Sodium nitroprusside	Sigma-Aldrich	PHR1423
<b>Critical commercial assays</b>		
RNAscope Manual Fluorescent Multiplex kit V2	Advanced Cell Diagnostics	323100
<b>Experimental models: Organisms/strains</b>		
Mouse, TRAP2	The Jackson Laboratory	030323
Mouse, Ai14	The Jackson Laboratory	007914
Mouse, EGFP-L10a	The Jackson Laboratory	024750
Mouse, Gad2-Cre	The Jackson Laboratory	010802
Mouse, ChAT-Cre	The Jackson Laboratory	006410
Mouse, Tac1-Cre	The Jackson Laboratory	021877
Mouse, Cartpt-Cre	from H. Zeng, Allen Institute for Brain Science	Jax stock no. 009615
Mouse, Th-Cre	European Mouse Mutant Archive	EM:00254

(Continued on next page)

**Continued**

REAGENT or RESOURCE	SOURCE	IDENTIFIER
<b>Oligonucleotides</b>		
eGFP <i>In situ</i> hybridization probe	Advanced Cell Diagnostics	400281
Slc17a6 <i>In situ</i> hybridization probe	Advanced Cell Diagnostics	319171
Slc32a1 <i>In situ</i> hybridization probe	Advanced Cell Diagnostics	319191
Chat <i>In situ</i> hybridization probe	Advanced Cell Diagnostics	408731
tdTomato <i>In situ</i> hybridization probe	Advanced Cell Diagnostics	317041
Cartpt <i>In situ</i> hybridization probe	Advanced Cell Diagnostics	432001
Adcyap <i>In situ</i> hybridization probe	Advanced Cell Diagnostics	405911
Nos1 <i>In situ</i> hybridization probe	Advanced Cell Diagnostics	437651
Pdyn <i>In situ</i> hybridization probe	Advanced Cell Diagnostics	318771
Gal <i>In situ</i> hybridization probe	Advanced Cell Diagnostics	400961
Tac1 <i>In situ</i> hybridization probe	Advanced Cell Diagnostics	410351
Cre <i>In situ</i> hybridization probe	Advanced Cell Diagnostics	312281
mCherry <i>In situ</i> hybridization probe	Advanced Cell Diagnostics	431201
Piezo1 <i>In situ</i> hybridization probe	Advanced Cell Diagnostics	500511
Piezo2 <i>In situ</i> hybridization probe	Advanced Cell Diagnostics	400191
Th <i>In situ</i> hybridization probe	Advanced Cell Diagnostics	317621
Gad2 <i>In situ</i> hybridization probe	Advanced Cell Diagnostics	415071
<b>Software and algorithms</b>		
MATLAB	MathWorks	R2016b, R2020a
OpenEx software	Tucker-Davis Technologies	N/A
Synapse	Tucker-Davis Technologies	N/A
ImageJ	NIH	<a href="https://imagej.nih.gov/ij/">https://imagej.nih.gov/ij/</a>
KlustaKwik	Kenneth D. Harris	<a href="http://klustakwik.sourceforge.net">http://klustakwik.sourceforge.net</a>
Ponemah	DSI	v 5.20
Bonsai	Neurophotometrics	FP3003 system
QuickNII	Puchades et al., 2019	<a href="https://www.nitrc.org/projects/quicknii;">https://www.nitrc.org/projects/quicknii/</a> ; RRID:SCR_016854
Ilastik	Berg et al., 2019	<a href="https://www.ilastik.org/">https://www.ilastik.org/</a>
Nutil Quantifier	Groeneboom et al., 2020; Yates et al., 2019	<a href="https://www.nitrc.org/projects/nutil/">https://www.nitrc.org/projects/nutil/</a>
Meshview	Groeneboom et al., 2020	<a href="https://www.nitrc.org/projects/meshview;">https://www.nitrc.org/projects/meshview/</a> ; SCR_017222

**RESOURCE AVAILABILITY****Lead contact**

Further information and requests for resources and reagents should be directed to and will be fulfilled by the lead contact, Yang Dan ([ydan@berkeley.edu](mailto:ydan@berkeley.edu)).

**Materials availability**

This study did not generate new unique reagents.

**Data and code availability**

All data necessary to understand and assess the conclusions of this manuscript are presented in the paper and the supplementary materials. The custom-written analysis codes and additional information required to reanalyze the data reported in this paper are available from the lead contact upon reasonable request.

**EXPERIMENTAL MODEL AND SUBJECT DETAILS**

Experiments were performed in adult male and female mice: TRAP2 (Jackson stock no. 030323), TRAP2 crossed with Ai14 (no.007914) or EGFP-L10a (no. 024750), Gad2-Cre (no. 010802), ChAT-Cre (no. 006410), Tac1-Cre (no. 021877), Cartpt-Cre (no. 009615, obtained from H. Zeng, Allen Institute for Brain Science), and Th-Cre (no. EM:00254, obtained from the European Mouse

Mutant Archive). Mice were housed in 12 hr light-dark cycle (lights on at 07:00 am and off at 07:00 pm) with free access to food and water. Animals with implants were housed individually. All procedures were approved by the Animal Care and Use Committee of the University of California, Berkeley.

## METHOD DETAILS

### Virus preparation

AAV2-EF1 $\alpha$ -DIO-ChR2-eYFP, AAV2-EF1 $\alpha$ -DIO-iC++-eYFP, AAV2-EF1 $\alpha$ -DIO-eYFP, AAV2-EF1 $\alpha$ -DIO-hM3D(Gq)-mCherry, AAV2-EF1 $\alpha$ -DIO-mCherry, AAV2-EF1 $\alpha$ -DIO-taCasp3-TEVp were obtained from the University of North Carolina (UNC) vector core. AAV2-hSyn-DIO-hM3D(Gq)-mCherry, AAV2-hSyn-DIO-mCherry, AAV9-CAG-FLEX-GCaMP6s-WPRE.SV40 were obtained from Addgene. AAV8-hSyn-FLEX-TVA-P2A-eGFP-2A-oG was purchased from the Gene Transfer, Targeting and Therapeutics Facility of Salk Institute for Biological Studies. RV- $\Delta$ G-mCherry was purchased from Gene Transfer Targeting and Therapeutics Core of Salk Institute, amplified in B7GG cells, pseudotyped with BHK-EnvA cells, and titered with HEK293-TVA cells ([Osakada and Callaway, 2013](#)). AAV2-CAG-FLEX-TC66T and AAV2-CAG-FLEX-RG (vector constructs were gifts from L. Luo) were prepared in house according to previously described protocols ([Hauswirth et al., 2000](#)). CVS N2c dG Histone-eGFP (H2BeGFP) rabies virus was obtained from A. Cetin and H. Zeng in the Allen Institute for Brain Science.

### Surgical procedures

Adult mice (6-12 weeks old) were anesthetized with 1.5%-2% isoflurane and placed on a stereotaxic frame. Body temperature was kept stable throughout the procedure using a heating pad.

For blood pressure and ECG telemetry recordings, the blood pressure probe (HD-X11, DSI, USA) was inserted into the left carotid artery caudal to the carotid bifurcation and advanced to position the pressure-sensing catheter tip in the aorta. The body of the telemetry device was placed subcutaneously in the left flank. The positive end of the ECG lead was placed in the left caudal rib region subcutaneously and the negative end was placed at the right pectoral muscle subcutaneously. For intravenous injection of drugs, a catheter was inserted into the right atrium through the right jugular vein ([Kmiotek et al., 2012](#)).

For EEG and EMG recordings, after asepsis the skin was incised to expose the skull, and the overlying connective tissue was removed. A reference screw was inserted into the skull on top of the left cerebellum. EEG recordings were made from two screws on top of the left and right cortex, at anteroposterior (AP) -3.5 mm, mediolateral (ML)  $\pm$ 3 mm. Two EMG electrodes were inserted into the neck musculature. Insulated leads from the EEG and EMG electrodes were soldered to a pin header, which was secured to the skull using dental cement.

For optogenetic activation/inactivation experiments, a craniotomy (0.5-1mm diameter) was made on top of the target regions (see below for coordinates), and 0.05 - 0.2  $\mu$ l virus was injected into the target regions using Nanoject II (Drummond Scientific) via a micro pipette. For the RVLM, AAV2-EF1 $\alpha$ -DIO-iC++-eYFP and AAV2-EF1 $\alpha$ -DIO-eYFP was injected bilaterally and into two AP positions on each side (see below for coordinates). Optic fibers (0.2 mm diameter; Thorlabs) were implanted into the target region with the tip 0.2-0.5 mm above the virus injection site two weeks after viral injection. Dental cement was applied to cover the exposed skull completely and to secure the implants for EEG and EMG recordings to the screws.

For chemogenetic activation of the NST, 0.2  $\mu$ l of AAV2-EF1 $\alpha$ /hSyn-DIO-hM3D(Gq)-mCherry was injected. For the Amb, 0.2  $\mu$ l of AAV2-EF1 $\alpha$ /hSyn-DIO-hM3D(Gq)-mCherry was injected into each of two AP positions (see below for coordinates). Recording devices (EEG, EMG, ECG and blood pressure) were implanted 2-3 weeks later.

For optrode recording experiments, a custom-made optrode assembly was inserted into the NST region. The optrode assembly was secured to the skull using dental cement.

For fiber photometry recording experiment, a craniotomy (0.5 -1mm in diameter) was made on top of the NST or the RVLM, and an optical fiber (200  $\mu$ m core, 0.37 NA, 1.25 mm ferrule, Neurophotometrics) was inserted into the region above the NST or the RVLM region.

For rabies-mediated retrograde transsynaptic tracing, 0.2  $\mu$ l of AAV8-hSyn-FLEX-TVA-P2A-eGFP-2A-oG was injected into the NST of TRAP2 and Cartpt-Cre mice. Three weeks later, 0.3  $\mu$ l of RV- $\Delta$ G-mCherry was injected into the same region. For the CVLM, 0.1-0.2  $\mu$ l of mixed AAV2-CAG-FLEX-TC66T and AAV2-CAG-FLEX-RG was injected into Gad2-Cre mice. Three weeks later, 0.2  $\mu$ l of CVS N2c dG Histone-eGFP (H2BeGFP) rabies virus was injected into the same region. For the RVLM, 0.2  $\mu$ l of mixed AAV2-CAG-FLEX-TC66T and AAV2-CAG-FLEX-RG was injected into each of two AP positions in Th-Cre mice. Three weeks later, 0.3  $\mu$ l of CVS N2c dG Histone-eGFP (H2BeGFP) rabies virus was injected into the same region. For the Amb, 0.2  $\mu$ l of mixed AAV2-CAG-FLEX-TC66T and AAV2-CAG-FLEX-RG was injected into each of two AP positions in ChAT-Cre mice. Three weeks later, 0.3  $\mu$ l of CVS N2c dG Histone-eGFP (H2BeGFP) rabies virus was injected into the same region. For all these experiments mice were sacrificed 5-6 days later for histology. Stereotaxic coordinates for virus injection and optic fiber implantation:

NST: anteroposterior (AP) -7.4 mm, mediolateral (ML) 0.5 mm, dorsoventral (DV) 5.0 mm (unilateral)

CVLM: AP -7.4 mm, ML 1.25 mm, DV 6.5 mm (ChR2: unilateral, iC++: bilateral, eYFP: bilateral)

RVLM: AP -6.8 and -7.2 mm, ML 1.3 mm, DV 6.5 mm (ChR2: unilateral, iC++: bilateral, eYFP: bilateral)

Amb: AP -6.9 and -7.4, ML 1.25 mm, DV 5.9 mm (unilateral)

Mice of specific genotype were randomly assigned to experimental and control groups. Experimental and control animals were subjected to exactly the same surgical and behavioral manipulations. Investigators were not blinded to animal identity and outcome assessment. After surgery, mice were allowed to recover for at least 1 week before experiments.

### TRAP induction

4-hydroxytamoxifen (4-OHT) was prepared based on K. Deisseroth's lab protocol. For PE-TRAP (IP2) and PE-TRAP (IP10), 4-OHT (2 mg/ml in saline with 2% Tween-80, 20 mg/kg) and PE (IP2: 2mg/kg, IP10: 10 mg/kg, P1240000, Sigma) were injected intraperitoneally concurrently. For PE-TRAP (IV), 4-OHT (2 mg/ml in saline with 2% Tween-80, 20 mg/kg) was injected intraperitoneally and PE (33-40 µg/kg/min) was intravenously infused for 1h. For Sal-TRAP, 4-OHT (2 mg/ml in saline with 2% Tween-80, 20 mg/kg) was injected intraperitoneally and saline was injected either intraperitoneally concurrently or intravenously infused for 1h. Mice were given at least 7 days to allow for expression before beginning experiments. In a subset of the mice, BP and ECG were recorded to confirm the effects of PE on cardiovascular activity. For optrode recording, optogenetic and chemogenetic manipulations performed in TRAP2 mice, AAV2-EF1 $\alpha$ -DIO-ChR2-eYFP or AAV2-EF1 $\alpha$ /hSyn-DIO-hM3D(Gq)-mCherry was injected into the NST 2-3 weeks before 4-OHT induction to allow virus expression. Recording devices (optrodes, EEG, EMG, ECG and blood pressure) were implanted >7 days after TRAP induction. To measure overlap between PE-TRAP (IP2: 2mg/kg, IP10: 10mg/kg) and PE-Fos, SNP-Fos and Sal-Fos, PE, SNP (0.6 mg/kg) or saline was injected intraperitoneally 40 min – 2 h before mice were sacrificed. To measure overlap between PE-TRAP (IV) and PE-Fos, SNP-Fos and Sal-Fos, PE (33-40 µg/kg/min), SNP (6.6-8 µg/kg/min) or saline was intravenously infused for 1 h.

### BP and ECG recordings

Telemetry recording of BP and HR was done in free-moving mice with a sampling rate of 1000 Hz or 2000 Hz (Ponemah v5.20, DSI, USA) according to the manufacturer's instructions. Baroreflex sensitivity was calculated as heart rate change divided by change in mean blood pressure 5 min after intraperitoneal injection of PE (2 mg/kg).

### Optrode recording

Custom-made optrodes consisted of an optic fiber (0.2 mm diameter) glued together with 6 pairs of stereotrodes. Two FeNiCr wires (Stablohm 675, California Fine Wire) were twisted together and electroplated to an impedance of ~ 200 kΩ using a custom-built plating device. The optrode was attached to a driver to allow vertical movement of the optrode assembly. A TDT RZ5 amplifier was used for the recordings, signals were filtered (0.3-8 kHz) and digitized at 25 kHz. At the end of the experiment, an electrolytic lesion was made by passing a current (100 mA, 10 s) through one or two electrodes to identify the end of the recording tract.

Spikes were sorted offline based on the waveform energy and the first three principal components of the spike waveform on each stereotrode channel. Single units were identified automatically using the software KlustaKwik (<http://klustakwik.sourceforge.net>). The quality of each unit was assessed by the presence of a refractory period and quantified using isolation distance and L-ratio. Units with an isolation distance < 20 and L-ratio > 0.1 were discarded.

To identify ChR2-tagged neurons, laser pulse trains (15 and 30 Hz with duration of 1 and 0.5 s, respectively) were delivered every 1 or 2 min. A unit was identified as ChR2 expressing if spikes were evoked by laser pulses with high reliability (> 0.4 for all units in our sample), short first-spike latency ( $\leq$  8 ms for all units in our sample), and the waveforms of the laser-evoked and spontaneous spikes were highly similar (correlation coefficient  $\geq$  0.98). To calculate the firing rate of each unit, spikes during the laser pulse trains were excluded.

To test whether unit activity was time-locked to heartbeats, we calculated the cross-covariance between binned (10 ms) firing rate and heart rate. To compute shuffled control, in each iteration the recorded spike train was shifted by a random time before computing the cross-covariance with the heart rate. For each experiment we computed 1000 shuffle covariance curves and the resultant distribution was used to compute confidence intervals for statistical comparison. To control for multiple comparisons, confidence intervals were Bonferroni corrected by the number of bins in the compared interval (e.g., to reach the significance level of  $p < 0.05$  with 40 comparisons within the window of  $\pm 200$  ms, the confidence intervals were plotted at  $1-0.05/40$ ). Cells with at least one time point surpassing the adjusted confidence level (99.9%) within the  $\pm 200$  ms time window were considered significantly time-locked.

### Polysomnographic recordings

Behavioral experiments were carried out in home cages placed in sound-attenuating boxes between 9:00 am and 7:00 pm. EEG and EMG electrodes were connected to flexible recording cables via a mini-connector. Recordings started after 20-30 min of habituation. The signals were recorded with a TDT RZ5 amplifier (bandpass filter, 1-750 Hz; sampling rate, 1,500 Hz). Spectral analysis was carried out using fast Fourier transform (FFT), and brain states were classified into NREM, REM and wake states (wake: desynchronized EEG and high EMG activity, NREM: synchronized EEG with high-amplitude, low-frequency (0.5-4 Hz) activity and low EMG activity, REM: high power at theta frequencies (6-9 Hz) and low EMG activity). The classification was made using a custom-written graphical user interface (programmed in MATLAB, MathWorks).

### Optogenetic manipulation

Each optic fiber was attached through an FC/PC adaptor to a 473-nm blue laser diode (LASERGLOW TECHNOLOGIES), and light pulses were generated using the TDT system. For all optogenetic experiments, constant light (1~2 mW at fiber tip) lasting for 120 s was used. In each optogenetic manipulation experiment, inter-trial interval was chosen randomly from a uniform distribution between 8 and 21 min, regardless of which brain state the animal was in. Each experimental session lasted for 3-5 hr and each animal was tested for 4-10 sessions. For activation of  $\text{NST}^{\text{PE-TRAP}}$  neurons, the ChR2-eYFP group includes 6 PE-TRAP(IP2) mice and 6 PE-TRAP(IV) mice, and the control group (expressing eYFP only) includes 2 PE-TRAP(IP2) mice and 4 PE-TRAP(IV) mice. For  $\text{NST}^{\text{CART}}$  neuron manipulation, the control group (expressing eYFP only) includes 6 mice, with BP and HR measured in 5 mice. In a subset of mice expressing ChR2-eYFP, laser (constant light, 120 s) was applied with 3 – 6 min intervals for 1 h before sacrifice, and FOS staining was performed to detect neurons activated by laser.

### Chemogenetic manipulation

Saline (0.9% NaCl) or CNO dissolved in saline was injected intraperitoneally (i.p.) into the corresponding Cre mice expressing hM3D(Gq) in the target region. CNO dose was 0.1 mg/kg body weight for activation in the NST and 1 mg/kg for Amb. For the control experiment (in mCherry-expressing mice), the same dose of CNO was administered for each region. Each recording session started immediately after injection. In each test set, mice were administered with saline and CNO in a random sequence (with CNO in the first day and saline in the second day or with saline in the first day and CNO in the second day, but always at the same time of the day between 12 and 2 pm). Each mouse was subjected to 2-4 test sets, and the data were averaged across all sets for each mouse. For activation of  $\text{NST}^{\text{PE-TRAP}}$  neurons, the Gq-mCherry group includes 6 PE-TRAP(IP2) mice and 5 PE-TRAP(IV) mice and the control group (expressing mCherry only) includes 6 TRAP(IP2) mice and 3 PE-TRAP(IV) mice with BP and HR measured in 6 mice. For  $\text{NST}^{\text{CART}}$  neuron manipulation, both the Gq-mCherry group and the control group (expressing mCherry only) include 6 mice each, with BP measured in 5 mice and HR in 6 mice. For Amb<sup>ChAT</sup> neuron manipulation, the Gq-mCherry group includes 15 mice with BP measured in 5 mice and HR in 11 mice and the control group (expressing mCherry only) includes 8 mice with BP measured in 4 mice and HR in 8 mice.

### Fiber photometry recording and analysis

Fiber photometry recording experiments started 2 weeks after surgical implantation of the fiber. The home cage of the mouse was transferred to the recording chamber and a fiberoptic patchcord (200- $\mu\text{m}$  core, 0.37 NA, 1.25 mm ferrule, low autofluorescence; Doric) was attached to the mouse's fiber implant using a ceramic split-sleeve (Thorlabs, Inc.). Fluorescent excitation was delivered using interleaved triggering of 470-nm and 405-nm LEDs (10-Hz trigger rate for each channel) and emission was measured with a Complementary Metal Oxide Semiconductor camera (FP3003 system; Neurophotometrics). Data were acquired using Bonsai (<https://open-ephys.org/bonsai>).

Photometry data were post-processed in MATLAB by first de-interleaving the 470-nm and 405-nm channels. Each channel was fit by a single-exponential decline to remove the changing baseline due to bleaching. The 405-nm channel was used to correct for any nonspecific changes in fluorescence, such as those due to movement artifacts. The 405-nm signal was fit to the 470-nm signal using least-squares linear fit (Lerner et al., 2015). After subtracting the fitted 405-nm signal from the 470-nm signal, the data were Z-scored at each time point relative to the total signal mean and standard deviation and used to analyze PE-induced activity change or brain state-related activity. Due to photobleaching, signals at the beginning of each recording (~30 min) were not used for analysis. For measuring PE-induced changes, each recording session lasted for 1-3 h with bolus saline or PE (1 mg/ml, 10  $\mu\text{l}$ ) injected intravenously for 2-6 times, and the baseline was defined as 100 s before injection to calculate dF/F. For measuring brain state-related activity, each recording session lasted for 3-5 h.

### Immunohistochemistry and fluorescence *in situ* hybridization (FISH)

Mice were deeply anaesthetized and transcardially perfused with 0.1M PBS followed by 4% paraformaldehyde (w/v) in PBS. For fixation, samples were kept overnight in 4% paraformaldehyde. For cryoprotection, samples were placed in 30% sucrose (w/v) in PBS solution for 36-48 hr. After embedding and freezing, brains were sectioned into 30- (*for FISH and a subset of immunohistochemistry*) or 50- $\mu\text{m}$  (*for other immunohistochemistry*) coronal slices and nodose ganglia were sectioned into 10- $\mu\text{m}$  slices using a cryostat. For immunohistochemistry, brain slices were washed using PBS three times, permeabilized using PBST (0.3% Triton X-100 in PBS) for 30 min and then incubated with blocking solution (5% normal goat serum or normal donkey serum in PBST) for 1 hr followed by primary antibody incubation overnight at 4 °C using anti-GFP (GFP-1020, Aves Labs, 1:500), anti-mCherry (M11217).

Life Technologies, 1:500) and anti-cFos (226003, SYNAPTIC SYSTEMS GMBH, 1:500) antibodies. Some brain slices were pre-treated for antigen retrieval. The next day, slices were washed with PBS and incubated with appropriate secondary antibodies for 2 hr (703-545-155, Alexa Fluor 488 donkey anti-chicken IgG, Jackson ImmunoResearch Lab Inc., 1:1000; A21209, Alexa Fluor 594 donkey anti-Rat IgG, Thermo Fisher Scientific, 1:1000; R37118, Alexa Fluor 488 donkey anti-rabbit IgG, Life Technologies, 1:1000; A21207, Alexa Fluor 594 donkey anti-rabbit IgG, Invitrogen, 1:1000). FISH was done using RNAscope Multiplex Fluorescent Assays V2 according to the manufacturer's instructions (Advanced Cell Diagnostics). To check Cre line specificity, FISH was performed followed by immunostaining. Fluorescence images were taken using a fluorescence microscope (Keyence BZ-X710) and a high-throughput slide scanner (Nanoozoomer-2.0RS, Hamamatsu).

**Whole-brain anatomical quantification**

For quantification of signals across the whole brain, brain areas were grouped into 12 brain structures according to the Allen Mouse Brain Atlas, but the olfactory bulb (OB) and the cerebellum (CB) were not shown, due to loss of tissue in the OB during dissection and high background noise in the CB. For NST input tracing, the nodose ganglion was included even though it is outside of the brain.

Whole-brain mapping of input neurons and output projections was performed by using QUINT ([Yates et al., 2019](#)). Briefly, the workflow contains 3 steps, 1) registration of brain section images to the 3D reference atlas by the QuickNII software ([Puchades et al., 2019](#)); 2) pixel and object classification by the *ilastik* software ([Berg et al., 2019](#)); 3) quantification by the *Nutil Quantifier* ([Groeneboom et al., 2020](#)). Signals were first detected automatically by *ilastik* and then validated manually by removing noise pixels (normally caused by the uneven auto-fluorescence of the brain tissue) after comparing the segmentation images with the original fluorescence image carefully. For RV tracing based on TVA in the NST, signals within ~1 mm radius of the injection site were excluded. For RV tracing based on TC66T in the Amb, CVLM and RVLM, starter cell signals were subtracted manually. The input was quantified as the number of RV cells in each brain region normalized by the total number of RV cells in each brain. The output (axon projection) to each region was quantified as the number of pixels occupied by detected axons in each brain region normalized by the total number of pixels detected in the whole brain.

Whole-brain mapping of PE-Fos was performed by the LifeCanvas Technologies. For whole-brain mapping of PE-TRAP, two samples were analyzed by LifeCanvas Technologies and one sample was analyzed using QUINT.

**QUANTIFICATION AND STATISTICAL ANALYSIS**

Data from all mice were included. Statistical analysis was performed using MATLAB and GraphPad. The brain state was scored with 5-s bins. Probability of each brain state in each time bin (before, during, after laser stimulation or following saline or CNO injection) was computed as the percentage of recording time spent in each state in that time bin; the probabilities for wake, NREM, and REM add up to 100% for all time bins. All statistical tests were two-sided. Data are shown as means ± SEM unless otherwise stated. The 95% confidence intervals (CI) for brain state probabilities were calculated using a bootstrap procedure: For an experimental group of  $n$  mice, with mouse  $i$  comprising  $m_i$  trials, we repeatedly resampled the data by randomly drawing for each mouse  $m_i$  trials (random sampling with replacement). For each of the 10,000 iterations, we recalculated the mean probabilities for each brain state across the  $n$  mice. The lower and upper confidence intervals were then extracted from the distribution of the resampled mean values. To test whether a given brain state is significantly modulated by laser stimulation, we calculated for each bootstrap iteration the difference between the mean probabilities during laser stimulation and the preceding period of identical duration. Two-way ANOVA with Bonferroni correction was used for comparisons of brain state between different conditions (saline or CNO) in chemogenetic experiments. For computing the neuron number and the overlap ratio of PE-TRAP neurons in the NST, neurons in the AP -7.0 to AP -7.8 were calculated. For other comparisons, tests were provided in the text or figure legends. For comparison between manipulated and control groups, data were checked for normality with Kolmogorov–Smirnov test; for normal distribution t-test was used, otherwise Mann–Whitney *U*-test was used. The “n” number for each experiment is provided in the text and figure legends. \* indicates  $p < 0.05$ , \*\*  $p < 0.01$ , and \*\*\*  $p < 0.001$ .